Conjugated polymer nanocomposites for bio-active nanoprobes

Seungyeon Hwang

The Graduate School

Yonsei University

Graduate Program for Nanomedical Science

Conjugated polymer nanocomposites for bio-active nanoprobes

A Dissertation

Submitted to the Graduate Program for Nanomedical Science

and the Graduate School of Yonsei University

in partial fulfillment of the

requirements for the degree of

Master of Science

Seungyeon Hwang

December 2014

This certifies that the dissertation of Seungyeon Hwang is approved.

[Thesis Supervisor: Seungjoo Hamm]

[Supervisory Committee: Jin-Suck Suh]

[Supervisory Committee: Jaemoon Yang]

The Graduate School

Yonsei University

December 2014

Contents

List of figures

Abstract

Conjugated polymer nanocomposites for bio-active nanoprobes

Seungyeon Hwang

Graduate Program for Nanomedical Science

The Graduate School

Yonsei University

In recent, conjugated polymers (CPs) have been reported as excellent sensing substrates due to its intrinsic opto-electric variability at each oxidation or reduction state. In particular, polyaniline (PAni) has attracted as a sensing material because of its easy synthesis, high conductivity, the controllable opto-electric property. Thus, PAni polyplex can perform as a suitable mediator of electron transfer in enzyme-based redox reactions for electro-chemical sensor. In addition, nano-sized PAni varies its color according to redox states by biological doping for bio-optical sensing. In this thesis, PAni nanocomposites were fabricated as a biomedical nanoprobe. First, porous PAni nanocomposite, named as PAni nanoskein (PANS), was synthesized using PAni and diverse solvents at sequential heating and cooling process. Interestingly, surface area-increased PANS was fabricated in a nanoscale with because of extraordinary polymer structure and solvent effect. Thus, PANS presented identifiable redox sensing potential by a biological doping for optical bio-active nanoprobe. On the other hand, for a detail diagnosis of cancer using magnetic resonance (MR) imaging, magnetic PAni nanohybrid (MPNH) was fabricated for a multi-sensing nanoprobe that it was consist of magnetic nanoparticle and PAni matrix. MPNH were synthesized by modified thermal decomposition method and then enveloped by amphiphilic surfactant to conjugate with

cancer targetable ligands. Thus, biomarker-targetable MPNH demonstrated potentials for optical redox state sensing and MR imaging for target cancer cells, simultaneously. In conclusion, PAni nanocomposites were designed and manufactured for a biomedical sensing. Due to opto-electric characteristics of PAni, PAni-based nanoprobes demonstrated redox-specific sensing activity for target cancer cells.

Keywords: Polyaniline • nanoprobe • nanoparticles • Magnetic resonance imaging • magnetic nanoparticle • biomarkers • conjugated polymer • diagnosis

Chapter I

Introduction

1.1. Nanoparticle in biomedical science

Nanoparticles have been attracted of many researchers, because it allows the study of the application in a variety ways. Nanoparticle has many advantages these are optical, chemical, and mechanical properties.[1, 2] Among them, chemical characteristic is representative advantages of the diagnostics, because nanoparticle can modify the surface that can use the bio-medical science. The modification of nanoparticle occurs the selectivity of disease, changes chemico-physical properties.[3, 4] Nanoparticle can take varied roles these are antigen detection, linker, fluorescent sensor, and drug deliver in medical nanotechnology. In detail, to aim the special site of diasease, the biomarker is available to use as a diagnostic agent. For instance, cyclic RGD is well known for typical biomarker of angiogenetic tumor vessel. The nanocomplex that is composed of magnetic nanoparticle and cyclic RGD can detect the angiogenetic tumor vessel using magnetic resonance imaging.[5]

On the other hand, nanoparticle has a larger surface area than other particles because it has small size.[6] This is an important meaning, and responsive to the large surface area, increasing as sensor detection of more sensitive. The sensitivity for accurate diagnosis is essential factor that can cause to build the effective treatment strategy. For example, the gold nanoparticles depending on the size and shape of the visible light in the area marked by laying surface plasmon resonance (SPR) breathing light and called the phenomenon observed. A little bit of nanoparticles SPR phenomenon, compared to the general fluorescent structures allocated to 4 ~ 5 times, as well as appear in the fluorescence photo-bleaching. Gold nanoparticles are surfacing in the biological material and coherent if SPR effect will grow gross color changes to the colorimetry, it is possible to use.[7]

See Figure I-1, nanoparticle performs a variety of functions, such as antigen detection, fluorescent signaling, biocompatibility, shape recognition and linkers in biomedical science. First of all, nanoparticle has the usability like as biosensor. E.g. Membrane type 1 metalloproteinase (MT1-MMP) significant attention for metastatic cancer therapy, because it was the one of transmembrane metalloproteinases that was expressed on the membrane on the invasive cancer cells. It is effective way to diagnose this antigen that the nanocompound is composed of magnetic nanoparticle and MT1-MMP biomarker. Because magnetic resonance imaging has advantages that it has high spatial resolution, multidirectional tomography, and anatomical images for accurate diagnosis.[8]

On the other hand, nanoparticle is used for fluorescent signaling agent a lot. Recently, nanoparticle surface energy transfer (NSET) effect has been studied many researchers, because it is useful characteristics for sensing agent of biomaterials. Fluorescein isothiocyanate (FITC) is representative fluorescent tracer to detect biomarkers. The gold nanoparticle that it has absorbance spectrum peak 500-530 nm can use as a quencher of FITC, FITC has emission peak spectrum peak wavelength of 519 nm. The gold nanocomplex conjugated with MT1-MMP cleavable peptide between gold nanoparticle and FITC is utilized to detect MT1-MMP using NSET effect.[7]

Biocompatibility is essential to be provided factor in biomedical science. In order to stably use the nanoparticle in biological application, various methods have been studied. Among them, surface-modified nanomaterial using surfactant is attracted many researchers. Polysorbate 80 has been used as amphiphilic surfactant that it can change hydrophobic phase to hydrophilic phase. In addition, Polysorbate 80 has been widly used in biomedical applications, because it has excellent bio-stability. In recent, some research has published those the hydroxyl groups of polysorbate 80 were substituted to other functional groups for extra originality of nanoparticles.[9]

These merits of nanoparticle are helpful to the evolution of biomedical science.

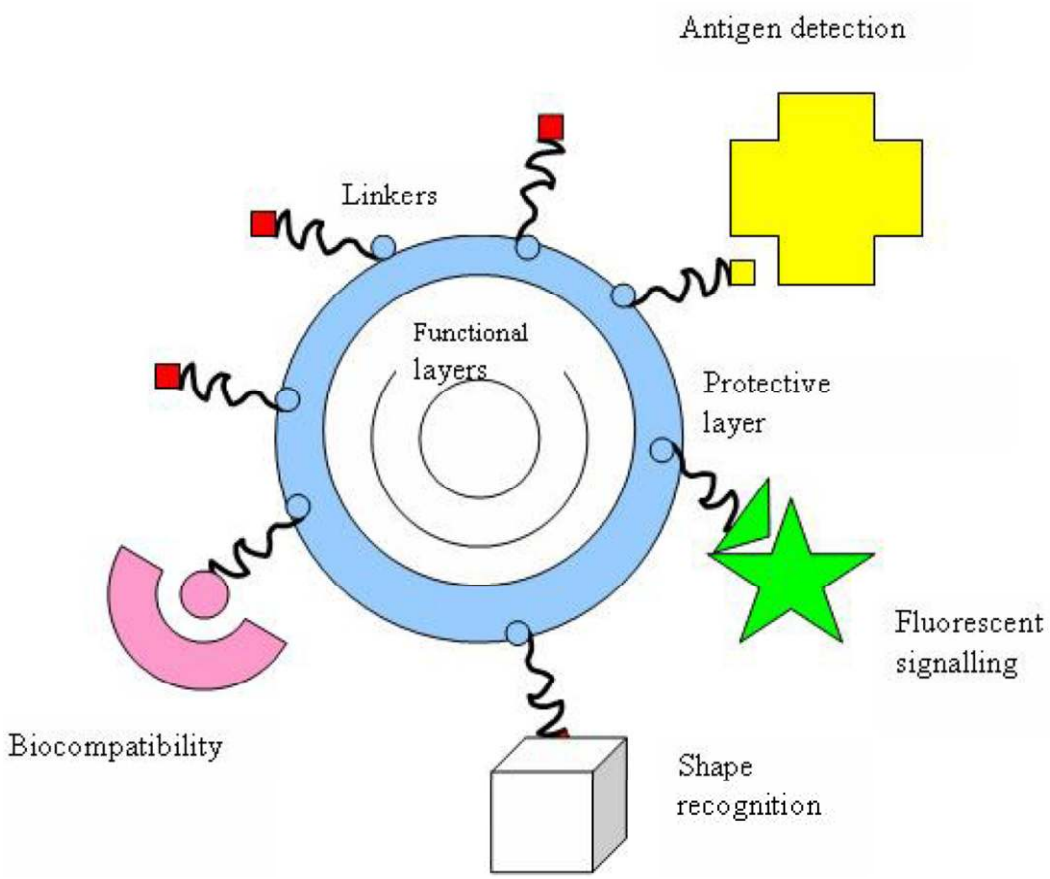

Figure I-1. Typical roles of nanoparticle in the biomedical technology. *J Nanobiotech*, 2004, **2**, 3

1.2. Necessity of redox sensing

Recently, redox sensing has been received lots of attention in biomedical researchers.[10-13] Oxidative stress, in general, is the phenomenon that it is not maintained the balance of antioxidant and oxidant, interfere with the normal physiological activity of the living body or the like is the cause of the disease.[14] Redox state is maintained by the balancing of the recovery and the defense mechanism of the oxidative damage caused by antioxidants, this balance is broken, causing a transformation and abnormal cell proliferation.[14-16] Herein, methods for detecting the redox by various ways in order to predict the occurrence and prognosis of cancer have been a lot of research. Among them, polyaniline (PAni) could be used to a redox sensing probe, because it

changed color under the reductable environment.[17, 18]

1.3. Polyaniline for biomedical science

Polyaniline (PAni) has been investigated as a conducting polymer, because it has a unique electrical property that can change by charge-transfer doping both the oxidation and reduction state. [19-21] Recently, PAni was suggested a new application for biomedical science that PAni could use as a biomaterials (Figure I-2).[17, 18] PAni has an opto-chemical property that it fluctuates with redox state, the color of solution by doping. To detect redox state in biological study is important, because it controls the cancer cell of growth and inhibition. PAni has advantage that PAni shows performance of detection redox state effectively.

On the other hand, PAni has another advantage that doped PAni has the absorbance at the infra-red region. It means doped PAni has another application such as photothermal agent, it can be absorbed the infra-red laser and heated the surrounding environment. PAni has these properties, which can be used for biomedical science.

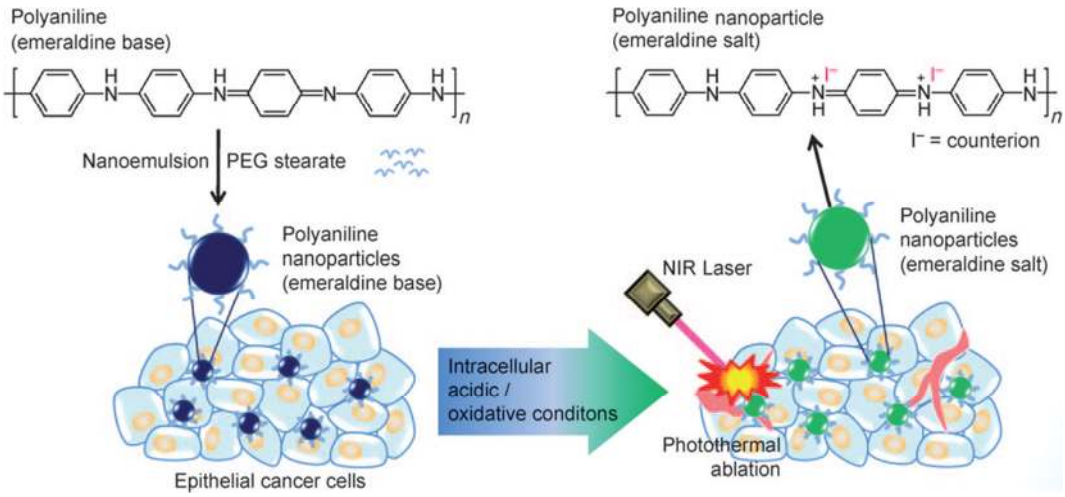

Figure I-2. Polyaniline in the biomedical science. *Angew Chem Int*, 2011, **50**, 442

Chapter II

Surface area enhanced optical probes of polyaniline nanoskein

Abstract

Recently, our group has reported that polyaniline (PAni) could be used to a redox sensing probe, because it changed color under the reductable environment. However, PAni had a problem to use biomedical sensing nanoprobe due to its hydrophobicity. Herein, we suggest a PAni nanoparticle that it has hydrophilic property and enhanced surface area, named as PAni nanoskein (PANS). PANS was manufactured using following process, adding benzyl ether, heating and cooling at room temperature, and then ethanol was added the mixture. To confirm chemical structure of PANS, FT-IR analysis was conducted, and the morphology was also observed by electron microscope. To demonstrate optical property of PANS, absorbance spectra were recorded. Finally, we verified that PANS has a possibility for biomedical sensing nanoprobes.

Keywords: Polyaniline • nanobiosensor • optical sensing • nanoparticle • scattering • photothermal • X-Ray photoelectron spectroscopy • Raman

2.1. Research background

A fundamental motivation for developments in flower-like shape nanoparticle has been incalculable attractions, because it shows unusual physical and chemical properties.[22, 23] In general, the three-dimensional materials, such as flower-shape nano-particles are composed of metal or metallic complex. These metallic flower-shape nanoparticles have the many ad-vantages, easy synthesis, different electrochemical properties, and abundant metallic surfaces.

On the other hand, polyaniline (PAni) nanoparticle has researched as metallic polymer nanoparticle, because PAni has valuable characteristics, easy synthesis, high conductivity, the reversibility of its oxidation/reduction processes, facile controllability of its redox state by doping.[24, 25] Consequently, PAni was already synthesized many synthesis method for nanostructures such as nanofibers, nanowires, and nanospheres.[26-30] Recently, PAni has reported nanoparticle for bio-sensor based on optical probe that it has different property of its redox state by doping, and the varying colors of its different redox states.[17, 18]

Now, we suggest the PAni nanoskein as optical nanoprobe. To confirm the chemical structure of PANS, first of all, Fourier transform infrared spectra were measured, and the shapes of 2-D and 3-D structures for PANS were also con-firmed via transmission electron microscopic and scanning electron microscopic images, respectively. The unique property of PAni, which is reversibility of color change as varying its doped state, is also shown in PANS. To demonstrate this characteristic, absorbance spectra were recorded as varying the pH of the surrounding solution, from pH 1 to 10. The PANS also showed a better potential for Raman agent than bulk PAni, and a near-infrared photothermal agent because of its high absorbance in near-infrared region. Collectively, in this work, we verified that PANS has a possibility of nanoprobe for biomedical applications as a photo-thermal and Raman agent, and to conclude, the PANS can sensitively and effectively detect redox state of surrounding environment.

2.2. Materials and Methods

2.2.1. Materials

Polyaniline (PAni) MW ~5,000 and benzyl ether were purchased from Sigma-Aldrich. 1-Methyl-2-Pyrrolidone (NMP) and ethanol (EtOH) were purchased from Dae-jung, KOREA. All other chemicals and reagents were analytical grade. Ultrapure deionized (DI) water was used for all of the synthetic processes.

2.2.2. Synthesis of PANS

The synthetic process of immaculate product was as follows: PAni (1 g) was dissolved in NMP (20 mL), than benzyl ether (20 mL) was added. The mixture was preheated to 200℃ for 1 hour and heated to 300℃ for 30 minutes. The reactant was cooled in room temperature for 3 hours. The resultant solution was washed with excess of EtOH, and separated the precipitant by centrifuging at 3,000 rpm for 10 minutes. Then, the solution was re-dispersed in EtOH. Next, the solution dissolved in EtOH was dialyzed using dialysis membrane (MWCO: 3,500 Spectra/Por® 6, SPECTRUM® LABORATORIES, INC) for 24 hours. After dialysis, the solution was centrifuged at 15,000 rpm for 30 minutes. The precipitant was re-dissolved in 30mL of DI water.

2.2.3. Characterization of PANS

The morphology and structure of PANS were evaluated with a transmission electron microscopic (TEM, JEM-1011, JEOL Ltd), and scanning electron microscopic (SEM, JSM-6701F, JEOL Ltd) imaging. X-ray photoelectron spectra were recorded using a Thermo U. K K-alpha system. Fourier transform infrared spectra (FT-IR Spectrum Two, Perkin Elmer) analysis was performed to confirm the characteristic bands of the synthesized PANS and the size distribution of the PANS

was analyzed by dynamic laser scattering (ELS-Z, Otsuka electronics) method. Furthermore, the surface area and pore volume of PANS was measured by Brunauer–Emmett–Teller analyzer (Autosorb-iQ 2ST/MP, Quantachrome) and the weight quantity of PANS was analyzed with a thermogravimetiric analyzer (SDT-Q600, TA instrument). Moreover, the absorbance of PANS was analyzed UV-vis spectrophotometer (Optizen 2120UV, MECASYS Co.) and light scattering images and spectra of single PANS were obtained using spectrograph coupled optical microscopic system. Finally, the photothermal effect was studied using thermo-coupled multimeter (FLUKE 289) and the Raman spectrum was obtained using Raman spectrometer (LabRam Aramis, Horriba Jovin Yvon).

2.3. Results and discussion

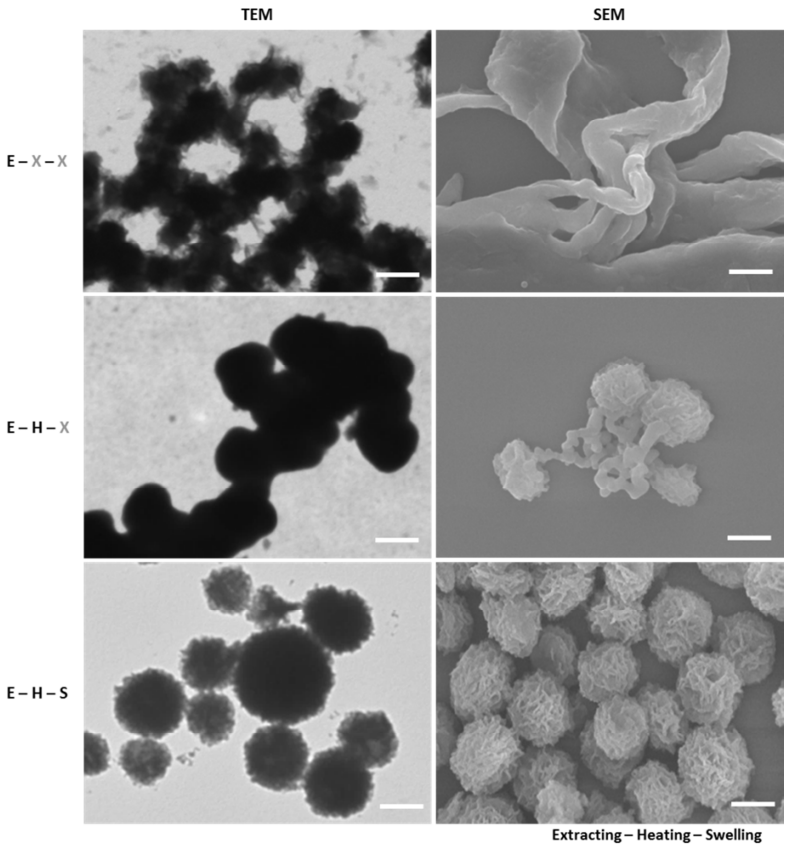

Figure II-1. Electron microscopic images of PANS (Scale bars: 500 nm). Alphabet characters mean; (E) Extracting with benzyl ether, (H) heating the mixture 200℃ and 300℃, (S) swelling the mixture using ethanol.

The morphology of the PANS was manifested by electron microscopy (Figure II-1). The PANS showed the spherical structure that it had irregular density in the particles. In order to synthesize of PANS, a variety of processes were used. PAni was dissolved NMP. BE was added into the PAni dissolved in NMP solution. Then PAni was precipitated by gap of solubility, because PAni had poor solubility in BE than NMP. The mixture was heated to the temperature over 200℃, precipitated PAni was condensed than previous process. The heated solution was cooled at room temperature. Ethanol was added into the cooled mixture, the precipitated PAni mixture was

swelled and formed like a skein. Each process of electron microscopic images were measured by (Figure II-2, 3). We poof the difference of PANS with PAni, PAni was dissolved in NMP, BE, ethanol. The electron microscopic images of dis-solved PAni various solvents were not equal to the morphology of PANS (Figure II-4). To find ideal synthetic condition of PANS, we synthesized PANS series using different molecular weight (MW) of PAni. The electron microscopic images of PANS various synthetic conditions show using MW 5,000 PAni was better than other conditions (Figure II-5).

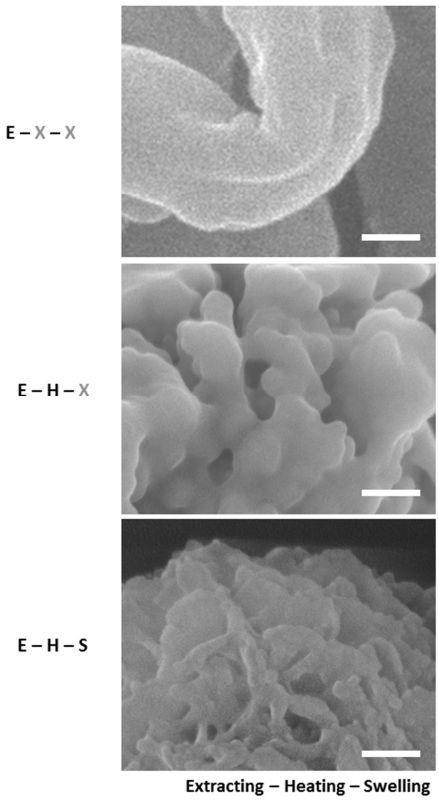

Figure II-2. FE-SEM images of PANS. Alphabetic characters represent sequential synthetic processes of PANS; (E): extracting reactant with benzyl ether, (H): heating sequentially the reactant at 200℃ and 300℃, and (S) swelling the reactant using ethanol. Scale bars are 100 nm.

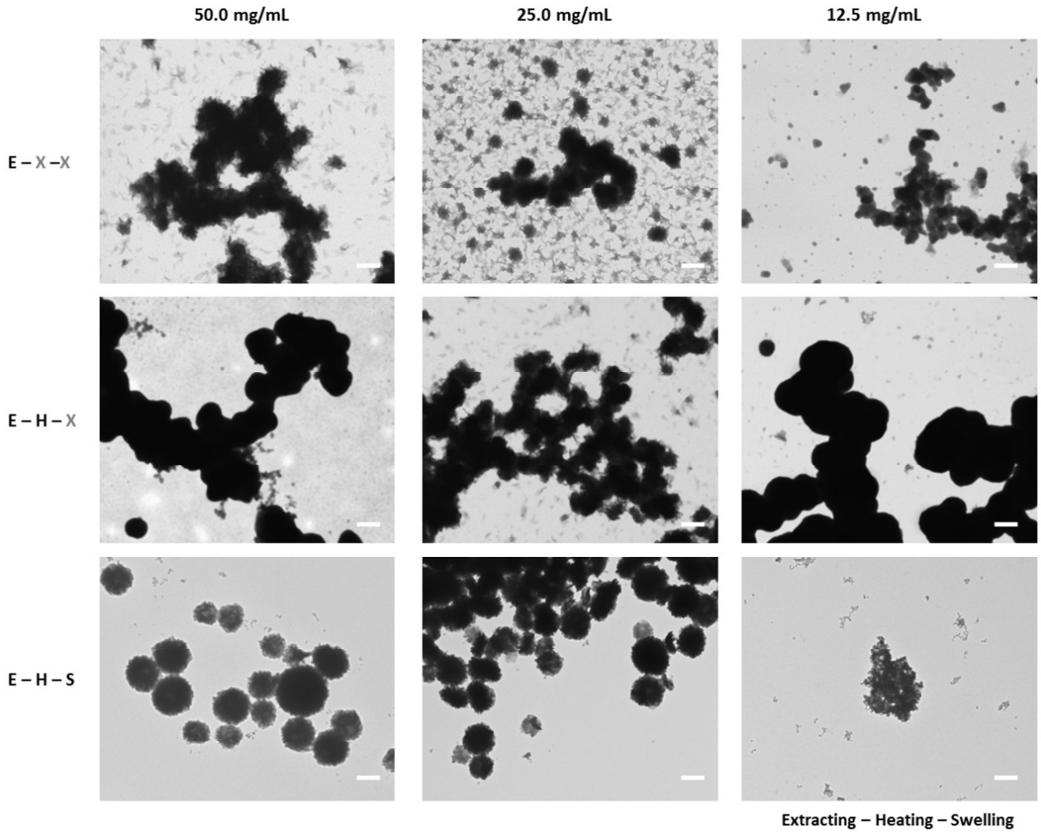

Figure II-3. TEM images of PANS according to changes of feeding amounts of PAni. Alphabetic characters represent sequential synthetic processes of PANS; (E): extracting reactant with benzyl ether, (H): heating sequentially the reactant at 200℃ and 300℃, and (S) swelling the reactant using ethanol. Scale bars are 500 nm.

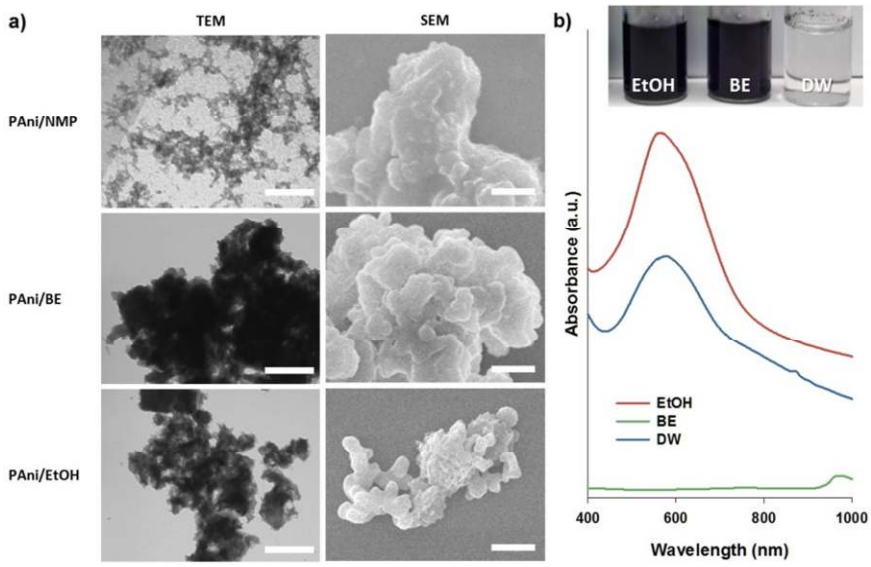

Figure II-4. a) TEM and SEM images of PAni just dispersed in indicated solvents. Scale bars are 500 nm. b) Absorbance spectra of PAni dispersed in indicated solvents. Inset is a photograph of PAni solutions dispersed in indicated solvents.

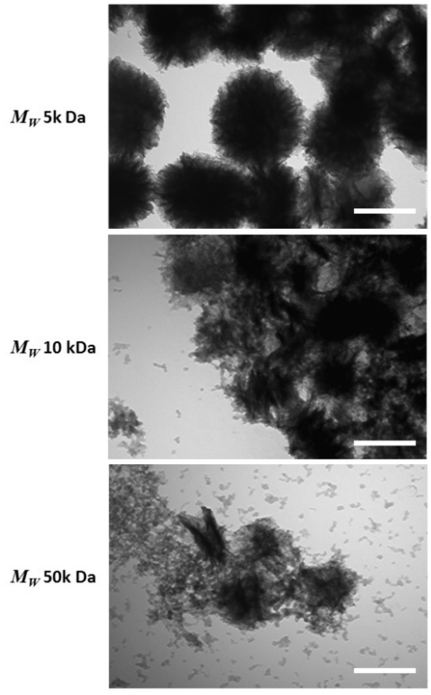

Figure II-5. TEM images of PANS according to changes of molecular weight (MW) of PAni. Scale bars are 200 nm.

As a shown Figure II-6, high resolution transmission electron microscopic image also shows that PANS has skein-like structure (Figure II-6a). In order to investigate the molecular structure of PANS, X-ray photoelectron spectroscopy (XPS) C (1s) core level spectra for bPAni and PANS were allowed. The spectra was deconvoluted as follows, C–C/C–H at 284.4 eV, C–N/C=N at 285.0 eV, C–N+/C=N+ 285.8 eV and C=O/C–O at 286.72 eV. PANS shows unlike in PAni. The integration ratios PAni : PANS of each peak is calculated, C–C/C–H 1 : 0.34, C–N/C=N 1 : 1.21, C–N+/C=N+ 1 : 1.56 and C=O/C–O 1 : 1.01 (Figure II-6b). This result means that the interaction is occurred between PAni to compose the PANS. The characteristic bands of PANS were verified by Fourier transform infrared (FT-IR) spectra: 1290 cm-1 (aromatic C-N stretching), 1488 cm-1 (C=C and C=N stretching of benzenoid ring), 1590 cm-1 (C=C and C=N stretching of quinoid ring), 1670 cm-1 (C=O stretching of carbonyl group; see Figure II-6c, Figure II-7). This FT-IR spectrum was revealed the fact that PANS has the functional groups such as bare polyaniline. Thermogravimetric analysis (TGA) of PANS display that it has another thing, besides PAni (Figure II-6d). The FT-IR and TGA results reveal that PANS was not pure PAni, PANS has the another materials that it has carbonyl group like NMP. Surface area and pore volume of PANS was determined by Brunauer–Emmett–Teller (BET) analyzer. The surface area of PANS was 9.486 m^2/g, bPAni was 6.358 m2/g, and the pore volume of PANS was 0.0440 cm3/g, bPAni was 0.0190 cm3/g. The BET results exhibit which PANS has more enhanced surface area and pore volume than PAni (Figure II-6e). The distribution of hydrodynamic diameter of PANS was measured by dynamic light scattering analyzer. The PANS display the size distribution of 799 ± 85 nm in an aqueous solution (Figure II-6f).

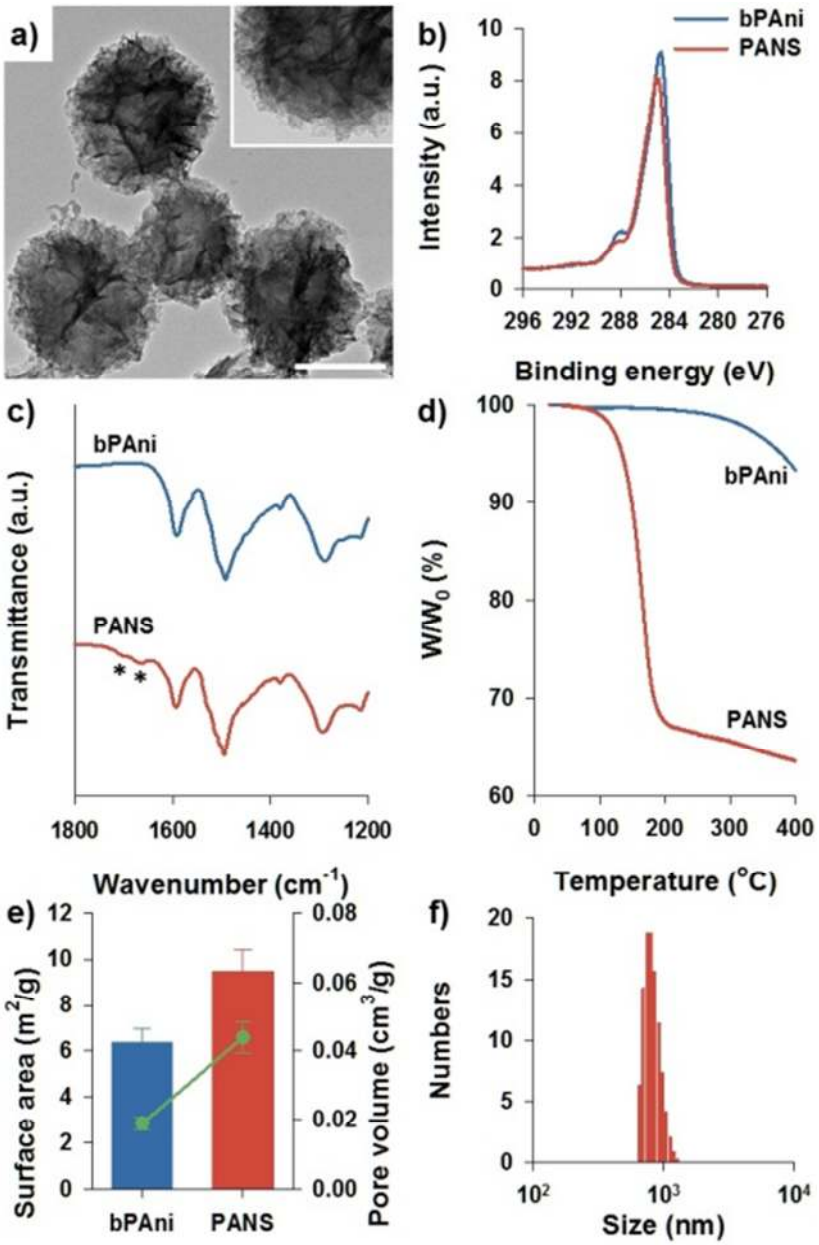

Figure II-6. a) Transmission electron microscopic images of PANS (Scale bars: 200 nm, insets: high magnification). b) C 1s XPS spectra of PANS (Scale bars: 100 nm). c) Fourier transform infrared spectra for bPAni (upper), PANS (lower). d) Thermogravimetric analysis of bPAni (upper), PANS (lower). e) BET surface area, pore volume of bPAni, and PANS. f) Size distribution of PANS.

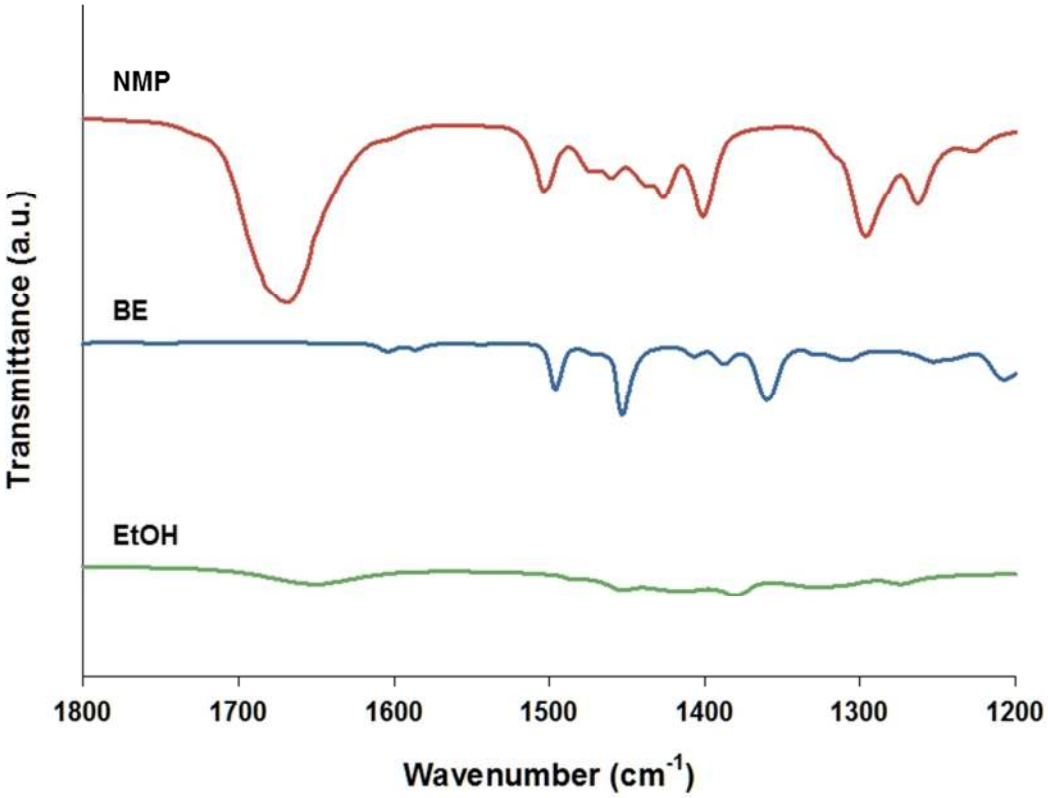

Figure II-7. FT-IR spectra for NMP, BE and EtOH.

To investigate the possibility of PANS such as optical probe, we confirmed optical property various method. In order to check the optical property of PANS by protonation, we test the absorbance of PANS in various pH conditions. First of all, the solution color of PANS changed lower pH to high pH, green to navy when pH was increased. The absorbance spectra of PANS in various pH conditions revealed the fact that PANS has similar property with PAni in pH changing (Figure II-8a, Figure II-9). In the low pH condition, the absorbance spectra showed red shift from 670 to 940 nm. This result suggests π-π* transition of benzenoid rings were detected in the absorbance spectra. To improve possibility of the colorimetric redox sensor, the darkfield image of PANS was measured (Figure II-8b upper inset). We also confirmed the PANS as a redox sensing nanoprobe, the scattering spectra of PANS were detected the absorbance gap at visible ray (Figure II-8b lower set, Figure II-10). On the other hand, PANS has high absoption in near infrared like as

the photothermal agent. So we tried the experiments that 808nm laser irradiation of the PANS in the doped and dedoped conditions (Figure II-8c, Figure II-11). The result of heat conversion efficiency was calculated that PANS in doping condition was higher than dedoping condition. The Raman spectra showed that PANS had same characterization with bare PAni, but Raman spectra ration on specific wavelength in each state showed that PANS could detect redox state using Raman spectrum analysis (Figure II-8d, Figure II-12).

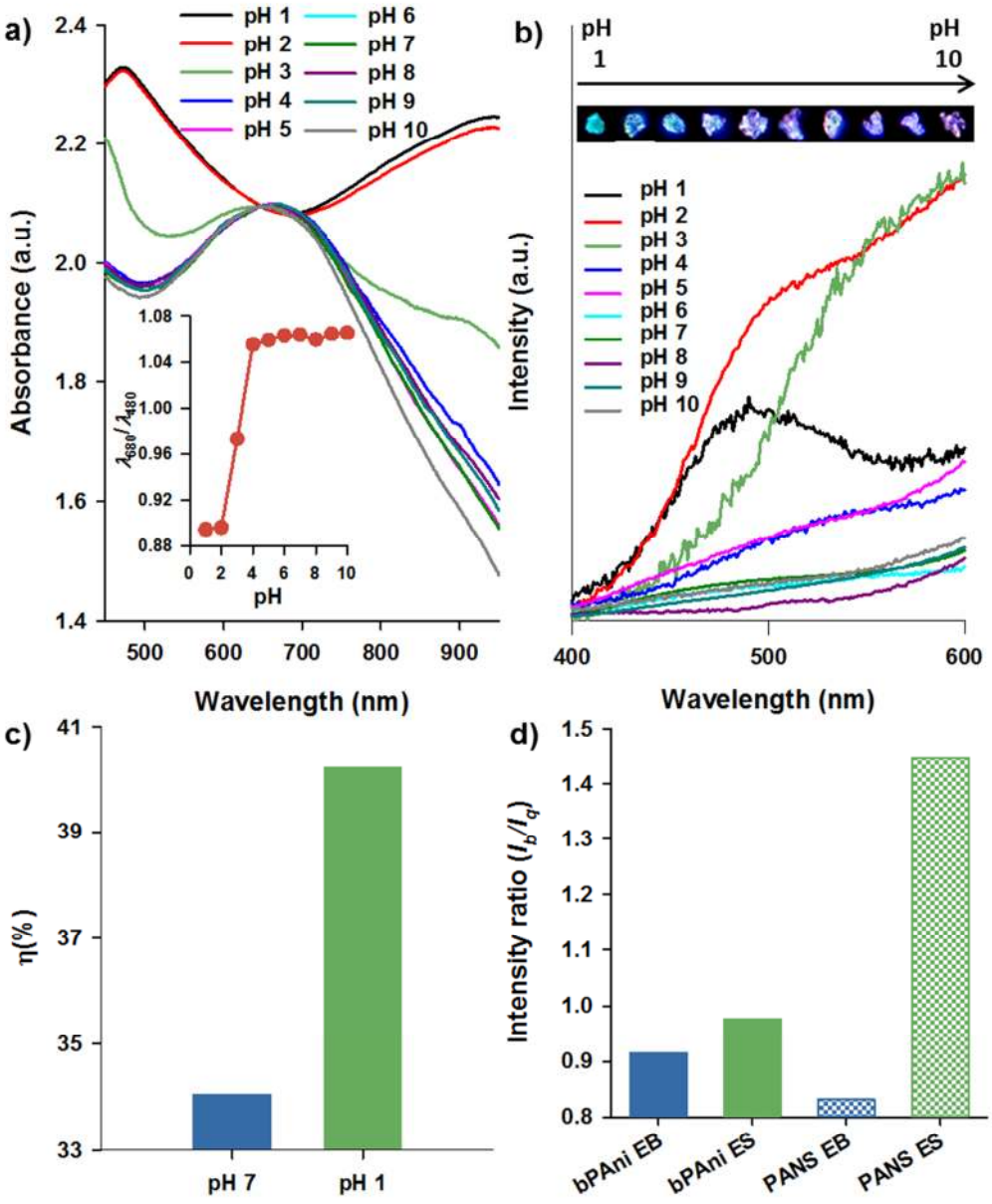

Figure II-8. Absorbance spectra of PANS in various pH solutions. The lower inset represents absorbance ratio for indicated wavelength. c) Heat conversion efficiency of PANS solution with pH1, pH7. d) Scattering spectra for single PANS. The upper inset represents darkfield image of PANS.

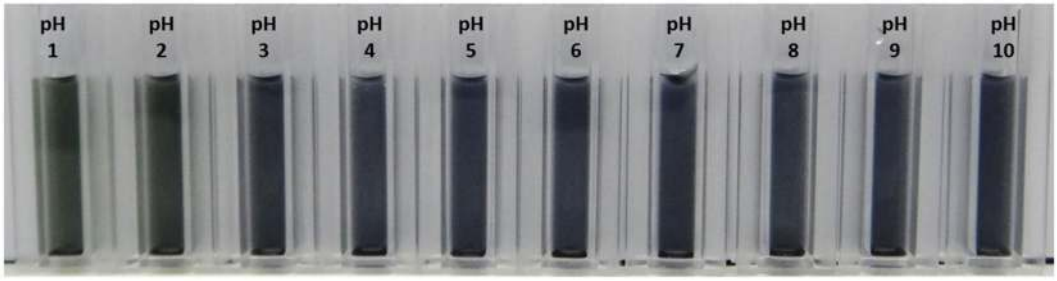

Figure II-9. Photograph of PANS solution in indicated pH conditions.

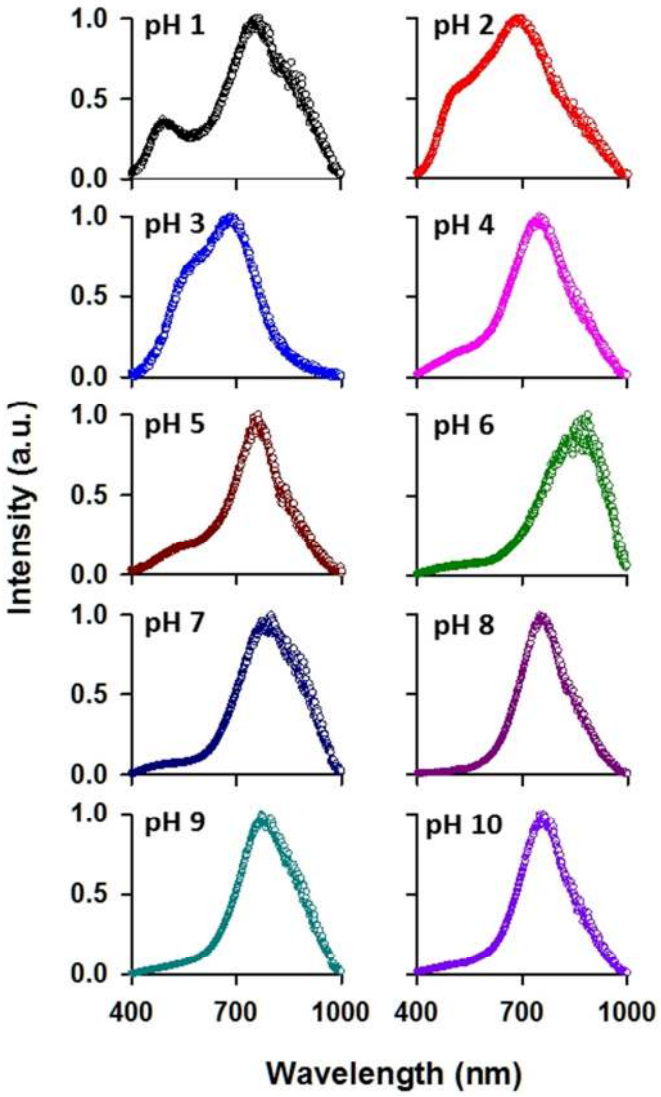

Figure II-10. Light scattering spectra of single PANS in indicated environmental pH conditions.

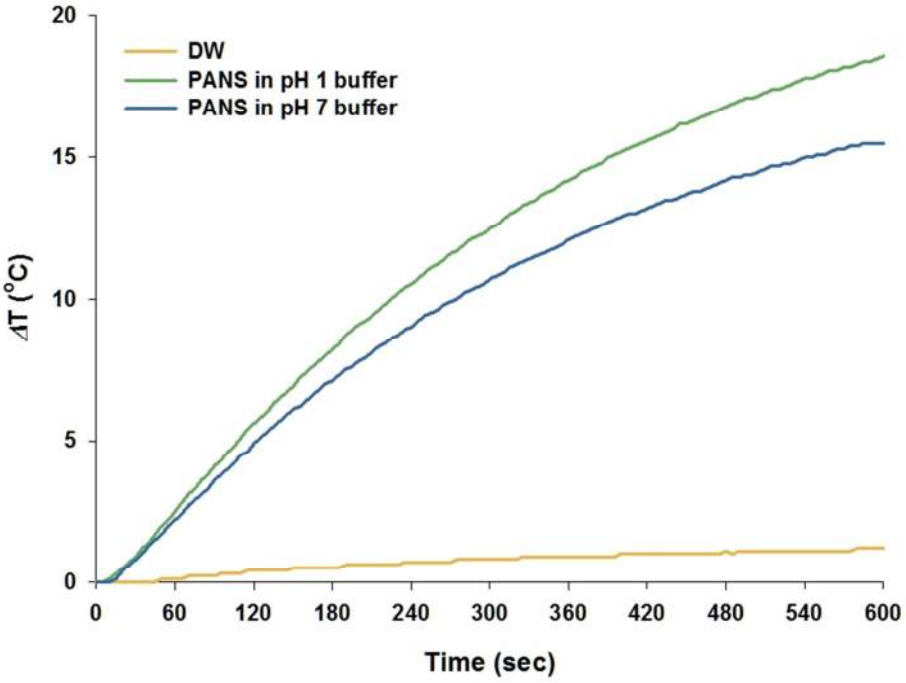

Figure II-11. Photothermal effect of the irradiation of DW, PANS in pH 1 buffer, and PANS in pH 7 buffer with an NIR laser (808 nm, 20 W/cm^2).

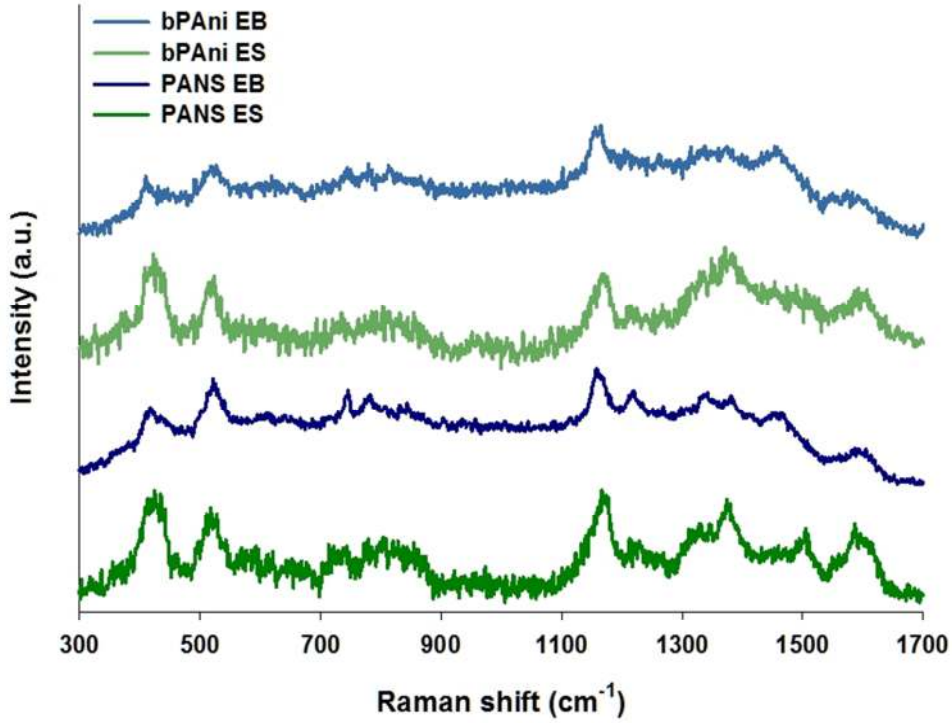

Figure II-12. Raman spectra of bPAni and PANS in EB and ES states, respectively.

2.4. Conclusion

In this study, we synthesized the PANS for redox-sensitive optical nanoprobe. PANS has high surface area with polyani-line, the skein-like spherical structure that it had many nano-size pores, and hydrophilic characteristics. PANS had same property with polyaniline, but it had many advantages as a optical nanoprobe. These results will contribute to the devel-opment of redox sensing optical physics, the PANS can play an important role.

Chapter III

Magnetic Polyaniline Nanohybrid for MR Imaging and Redox Sensing of Cancer Cells

Abstract

In recent, polyaniline has been used as a redox sensing agent in our research group, because it can change the color under the reductable environment. To diagnose cancer cell, on the other hand, magnetic nanoparticles have used in magnetic resonance (MR) imaging agents. From these facts, we synthesized a magnetic polyaniline nanohybrid (MPNH) for redox sensing agent guided by MR imaging. MPNH was synthesized using iron-acetylacetonate and polyaniline by thermal-decomposition method without any additive ligands. To detect membrane type 1 metalloproteinase (MT1-MMP), subsequently, the surface of MPNH was PEGylated and modified with MT1-MMP-specific targetable peptide. To estimate MR imaging potential and redox sensing capability of MPNH for target cancer cell, MPNH was intravenously injected into the tumor-bearing mice. Finally, we found the possibility that MPNH had valuable advantages for metastatic cancer diagnostic agents and specific targetable agents.

Keywords: polyaniline • magnetic nanoparticle • nanohybrid • cancer • molecular imaging • redox-state

3.1. Research background

Recently, multifunctional nanostructures have been designed by researchers.[31-34] In particular, magnetic nanoparticles (MNPs) composed of iron have been used for magnetic resonance (MR) imaging as a drug delivery carrier.[31] MR imaging potential of MNPs occurs from its remagnetization response to a magnetic field.[35] On the other hand, one of the most reported conducting polymers, polyaniline (PAni), has attracted significant interest due to its easy synthesis, high conductivity, reversibility of its oxidation/reduction processes, facile controllability of its redox state by doping, and varying colors of its different redox states.[17, 18] PAni is especially interesting as a material for biosensors, because it can act as an effective mediator for electron transfer in redox and enzymatic reactions.[36] The role of PAni as a mediator is due to the presence of delocalized redox charges over a series of conducting grains (polarons) in its crystallite emeraldine salt-I phase.[37] PAni is considered to be an attractive polymer, since it exhibits two redox couples in the appropriate range to facilitate an enzyme-polymer charge transfer and thereby acts as a self-contained electron transfer mediator.

Herein, we suggest the use of bifunctionally magnetic PAni nanohybrids (MPNHs) for MR imaging and redox sensing of the cancer cell microenvironment. MPNHs are consisted MNPs that function as MR contrast agents, and PAni acts as a redox-sensing agent. The sensing of the redox state in biological systems occurs because the redox state is related to the regulation of protein activity, cell signaling, gene transcription, and various cellular events in response to reactive oxygen species.[38-41] To synthesize water-soluble nanoprobes, MPNHs are functionalized with maleimidyl-TWEEN 80 (MPNHm), and MPNHm shows potential as an MR contrast agent by solution MR imaging. Moreover, the synthesized MPNHm shows reversibility of its color changes with changing pH condition, as also an original characteristic of PAni. Subsequently, MPNHm was conjugated with a peptide (MPNHm-P), which can be targeted toward one of the representative biomarkers of invasive cancer cells, membrane type 1-matrix metalloproteinase (MT1-MMP). MPNHm-P confirmed the redox-sensing potential and targeting ability in an MT1-MMP-

overexpressing cell line (HT1080) compared to a low-expressing cell line (MCF7). Furthermore, MPNHm-P was injected into tumor site of a xenograft mouse model directly, In vivo MR and optics images were used to show the potential of the MR contrast agent and redox-sensing agent, respectively (Figure III-1).

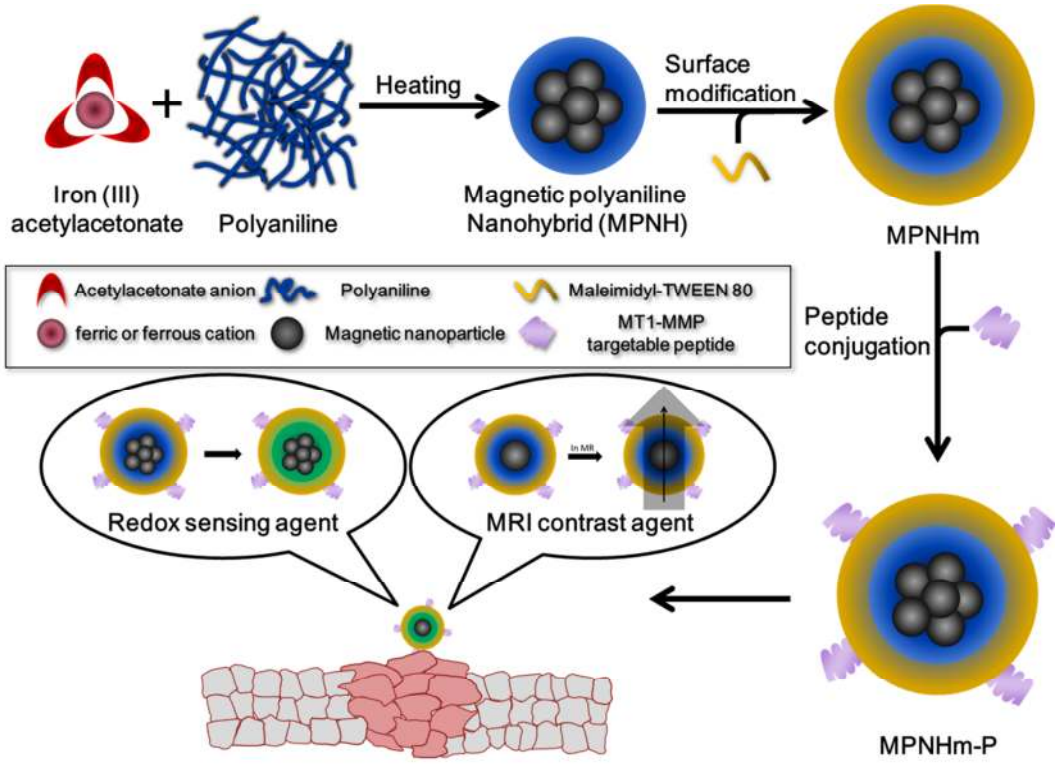

Figure III-1. Schematic illustration of the synthesis of a magnetic polyaniline nanohybrid (MPNH) as an MR imaging and redox-sensing agent.

3.2. Materials and methods

3.2.1. Materials

Polyaniline (PAni, 5,000 Da), benzyl ether, Tween 80, dichloromethane, and Iron (III) acetylacetonate were purchased from Sigma-Aldrich (St. Louis, MO, USA). 3-maleimidopropionic acid is purchased from Tokyo Chemical Industry Ltd, and membrane type-1 matrix metalloproteinase (MT1-MMP) targetable peptide is obtained from Peptron. 1-Methyl-2-Pyrrolidone (NMP) and ethanol (EtOH) were purchased from Dae-Jung, KOREA. All other chemicals and reagents were analytical grade. Ultrapure deionized water (DW) was used for all of the synthetic processes.

3.2.2. Synthesis of polyaniline-coated magnetic nanohybrid (PMNH)

The synthetic process of immaculate product was as follows: 1g of PAni was dissolved in 20 mL of NMP. 706.4 mg iron (III) acetylacetonate was dissolved in 20 mL of benzyl ether. After mixing of the two solutions, then the mixture was pre-heated to 200^{o}C for 1 hour, repeatedly heated to 300^{o}C for 30 minutes. The reactant was cooled in room temperature for 3 hours. Subsequently, the product was washed with excess of EtOH, and separated the precipitants by centrifuging at 3,000 rpm for 10 minutes. This centrifugation was repeated for three times, and then, the product was re-dispersed in EtOH. The end product was dispersed in NMP. After synthesis of PMNH, the morphology and structure of PMNH were evaluated with a transmission electron microscope (TEM, JEM-1011, JEOL Ltd). Fourier transform infrared spectra (FT-IR spectrum Two, Perkin Elmer) analysis was performed to confirm the characteristic bands of the synthesized PMNH. The absorbance of PMNH was analyzed UV-Vis spectrophotometer (Optizen 2120UV, MECASYS Co.).

3.2.3. Preparation of maleimide modification of TWEEN80.

1 g of TWEEN80 was dissolved in 50 mL of dichloromethane. 0.709 g of N,N'-dicyclohexylcarbodiimide, 0.420 g of 4-dimethylaminopyridine, 0.194 g of 3-maleimidopropionic acid, and 0.479 mL of triethylamine were added the solution, respectively. The mixed solution was stirred for 48 hours at the room temperature. The unwanted solution was rapidly removed using the rotary evaporator. The product was re-dissolved in DW, and then dialyzed excess deionized water (DW) for 24 hours. After dialysis, the mixture was filtered using filter paper to remove the unwanted precipitate. Finally, the product was freeze-dried and stored.

3.2.4. Preparation of PMNHm and PMNHm-P.

0.1 g of maleimido-modified TWEEN80 was dissolved in 30 mL of DW. 5 mL of PMNH solution was added and magnetic stirred for 4 hours at the room temperature. The product was re-dissolved in DW, and then dialyzed excess DW for 2 days.and then dialyzed excess DW for 2 days. 450 μg of MT1-MMP targetable peptide was dissolved into the 5 mL of PMNHm solution. Then, the solution mixed using a vortex for 30 minutes. After synthesis of PMNHm, the morphology and structure of PMNHm were analyzed by Transmission electron microscopy. The hydrodynamic size and zeta potential were measured using dynamic light scattering method and the presence and crystallinity of magnetic substances in the PMNHm was verified using X-ray diffraction analysis. The sensitivity toward a magnetic field was investigated using vibrating sample magnetometer. MR imaging of PMNHm experiments were performed with a 1.5-Tesla clinical MRI instrument with a Micro-47 surface coil (Intera, Philips Medical Systems). R2 relaxivities of PMNHm solutions were measured at room temperature with the Carr-Purcell-Meiboom-Gill sequence (TR = 400 ms, 32 echoes with 12-ms even echo space, number of acquisitions = 1, point resolution = 0.234 × 0.234 mm, section thickness = 0.6 mm). R2 was defined as 1/T2 with units of s^{-1}. The ratio of R2 to PMNHm concentration is equal to the relaxivity coefficient (mM^{-1} s^{-1})

3.2.5. Cell culture conditions and viability study.

Human breast cancer, MCF7, and fibrosarcoma, HT1080 cell lines were cultured in DMEM with 10% fetal bovine serum in a humidified incubator containing 5% CO_2 at 37^{o}C. The cell viability of PMNHm-P for HT1080 and MCF7 cells were quantified by a colorimetric assay based on the mitochondrial oxidation of 3-(4, 5-dimethylthiazoly-2)-2, 5-diphenyltetrazolium bromide (MTT) (Cell Proliferation Kit I, Roche, Germany). In a typical cell viability experiment, HT1080 cells and MCF7 cells (1×104 cells/well, respectively) were seeded into 96-well plate and incubated at 37^{o}C in a 5% CO2 atmosphere. The cells were incubated for 4 hours with PMNHm-P, and after 24 hours, the yellow MTT solution was treated, and the formed formazan crystals were solubilized with 10% sodium dodecyl sulfate in 0.01 M HCl. Then the absorbance of the resulting colored solution was measured at 584 nm and at 650 nm as a reference using a microplate spectrophotometer (EpochTM, BioTek, USA). Cell viability was determined from the intensity ratio of treated to non-treated control cells and shown as an average ± standard deviation (n = 4).

3.2.6. In vitro redox-sensing.

To measure the absorbance of PMNHm-P in cells, HT1080 cells and MCF7 cells (1×104 cells) incubated with 3.17 mM of PMNHm-P, that is, non-toxic concentration (based on iron concentration) were moved into cuvette. The cuvette was mounted on our home built absorbance measurement system between a quartz-tungsten-halogen light source (Ocean Optics, HL2000) with focusing lens and a portable spectrometer (Ocean Optics, USB4000) with collimating lens. For dark field imaging of cells with PMNHm-P, scattering imaging system was used. The imaging system was composed of an inverted microscope (Axio Observer A1, Carl Zeiss) and a color CCD camera (DCU224C, Thorlabs).

3.2.7. In vivo model and MR imaging.

All animal experiments were conducted with the approval of the Association for Assessment and Accreditation of Laboratory Animal Care International. To establish the orthotopic mouse model of fibrosarcoma, HT1080 cells (5.0×10^6 cells) were implanted into the proximal thigh of female mice (6-week-old BALB/c-nude mice). When tumor size reached approximately 500 mm^3 (tumor volume in mm3 is calculated by following formula, tumor volume = $4/3 \times \pi \times (width/2)^2 \times (length/2)^2$), PMNHm-P was injected intravenously into the tail vein. *In vivo* MR imaging experiments were performed with a 3.0 T clinical MRI instrument (SIMENS). For T2-weighted MR imaging, the following parameters were adopted: TR = 3,000 ms even echo space, number of acquisitions = 4, point resolution of 192 × 180 mm, section thickness of 0.1 mm and TE = 79 ms.

3.2.8. Tissue staining and imaging.

After in vivo MR imaging, hematoxylin and eosin (H&E) and Prussian blue staining were conducted to confirmation of PMNHm-P targeting for MT1-MMP-expressing on HT1080 cancer cells. Tissues were embedded in paraffin after being dehydrated in increasing alcohol concentrations and cleared in xylene. Slices (thickness = 10 μm) were mounted onto glass slides and were twice placed in a container filled with hematoxylin for 10 minutes, to stain the nuclei. Tissues were rinsed in water for 10 minutes to remove hematoxylin, and the cytoplasm was stained with eosin and dehydrated in the same method as described above. After washing three times for 30 minutes, we added 2 ~ 3 drops of the mount medium onto the slide and then covered the slide with a cover slip. To visualize the existence of PMNHm-P on tumor, an additional slide was stained using the Prussian blue staining kit. All of the stained tissue sections were analyzed using a virtual microscope (Olympus BX51, Japan) and Olyvia software.

3.3. Results and discussion

To verify the fabrication of MPNHs in steady state, transmission electron microscopy (TEM) imaging was preferentially conducted. Figure III-2a-d show TEM images of MPNHs synthesized by various molar ratios of iron (III), acetylacetonate (I), and PAni (P). In Figure 1a, without using PAni (I : P = 10 : 0), single MNPs, of 10.3 ± 4.3 nm were irregularly clustered and showed no PAni coating. In Figure 1b, an increased molar ratio of PAni (I : P = 10 : 0.25) induced the regular self-assembly of single MNPs with PAni coating and showed a narrow size distribution of MPNHs of 71.3 ± 5.6 nm. In Figure 1c, it can be seen that the clustering tendency between single MNPs decreased, and MPNHs were losing their spherical shapes due to the increased PAni molar ratio (I : P = 10 : 0.75). In Figure 1d (I : P = 10 : 1), the spherical shape of the particles was not found by TEM, and MPNHs formed a large area of the PAni cloud containing MNPs. From these results, we decided that the conditions in Figure 1b were ideal for the synthesis of MPNHs, and the following experiments were conducted using this approach. The presence of PAni in MPNHs was shown using a solubility test for MPNHs using deionized water (DW), ethanol (EtOH), and N-methyl-2-pyrrolidone (NMP). As described in Figure III-2e, with either DW or EtOH, MPNHs had poor solubility, aggregated, and precipitated. In contrast to this result, with NMP, MPNHs were well dispersed and had a higher solubility than either DW or EtOH. These effects seem to be caused by one of the representative characteristics of PAni, which involves MNP. As described in a previously published report,8 PAni has better solubility in NMP than in DW, and we also observe this solubility property in MPNHs. The absorbance spectra also show the presence of PAni as well as the solubility of MPNHs toward DW, EtOH, and NMP. Because of the aggregation and precipitation of MPNHs in DW and EtOH, the absorbance spectra of MPNHs in those cases cannot be measured, but in NMP, the proper absorbance spectrum can acquired. These results are proof for the involvement of PAni with MNP, and are consistent with a previously published report.4 The chemical structure of MPNHs was confirmed by peaks in the Fourier transform infrared (FTIR) spectra: 1580 cm-1 (C=C and N=Q=N stretching of the quinoid ring, denoted as i),

1400 and 1495 cm-1 (C=N stretching of the quinoid ring, denoted as ii), and 1300 cm-1 (aromatic C-N stretching of bezenoid rings, denoted as iii) (Figure III-2f). The results in Figure 1 show that MPNHs can be successfully fabricated in a nanohybrid form, and PAni is well contained in the MPNH as we expected.

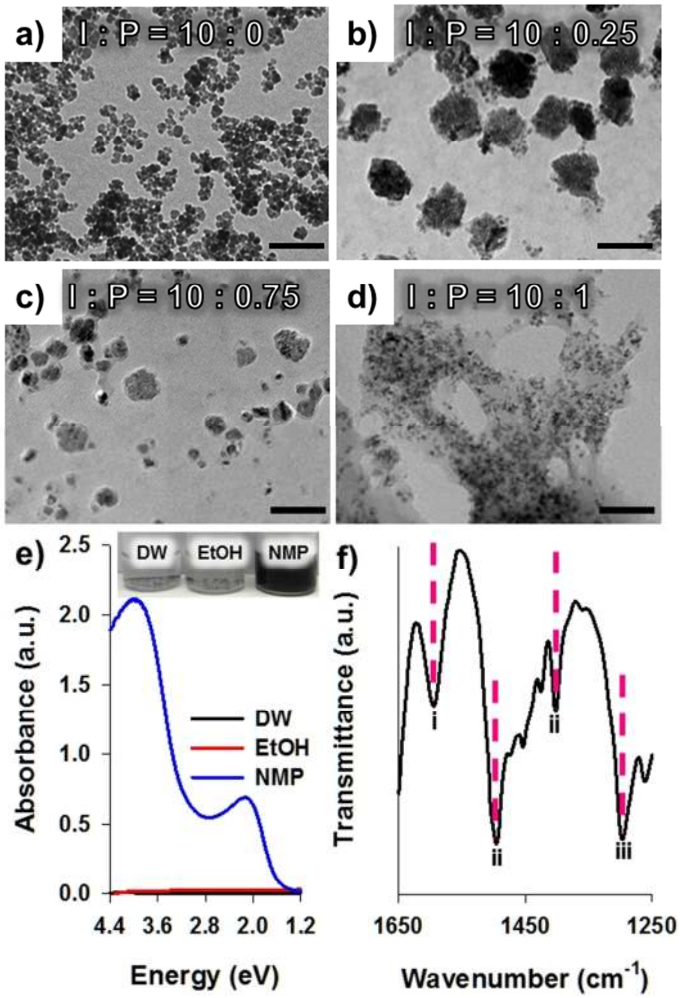

Figure III-2. TEM images of MPNHs under the following ratios for iron (I) and polyaniline (P): a) 10:0, b) 10:0.25, c) 10:0.75, and d) 10:1. e) Absorbance spectra for MPNHs dispersed in the indicated solvents. Inset is a photograph for solutions containing polyaniline in the indicated solvents. f) FTIR spectra for MPNHs. The Roman characters (i, ii, and iii) represent interesting peaks described in more detail in the text.

In order to increase the capability of MPNHs as MR contrast agents and redox-sensing agents in biological systems, a nano-precipitation method was applied to improve the solubility and stability of MPNHs in water.8 Maleimidyl-TWEEN 80 was used as a surfactant; as a result, the surface of the MPNH was modified with a maleimidyl group (MPNHm). To investigate the influence of the doping property by PAni, the MPNHm was doped using various pH solutions (pH 1 ~ 10). Figure III-3a shows the effect of pH on the optical properties of the MPNHm. At low pH (< pH 2), MPNHm was converted into the ES (green color) state. At higher pH (> pH 3), MPNHm transitioned to an EB state (blue color). The absorbance spectra of MPNHm over a range of pH values were measured (Figure III-3b). At pH 1, PAni nanoparticles were in the doped state (ES), as indicated by the presence of the π–π* transition of the benzenoid rings as well as the polaron band transitions at about 2.95 and 1.30–1.55 eV. With decreasing HCl concentrations, the polaron bands at 2.95 and 1.30–1.55 eV gradually decreased in intensity, and a strong absorbance band at about 2.14 eV was observed. The absorbance band at 2.14 eV is attributed to excitation from the highest occupied molecular orbital of the three-ring benzenoid structure of PAni to the lowest unoccupied molecular orbital of the localized quinoid ring and the two surrounding imine nitrogens in the EB state of the PAni nanoparticles. In order to distinguish more quantitatively between the EB and ES states of MPNHm, the absorbance ratios (E1.55/E2.14) were calculated at the representative energies of the peaks for the EB (E1.55) and ES (E2.14) states (Figure III-3c). As the pH value increased from 1 to 6, the absorbance ratio also decreased, but it did not change further at the higher pH value (> pH 7). Additionally, to confirm the capability of redox sensing of MPNHm in biological systems, scattering spectra of a single MPNHm molecule were measured, and darkfield imaging of MPNHm was also conducted by varying the pH. As shown in Figure 2c, scattering intensity ratios dramatically transited between pH 2 and pH 3. Visualizing darkfield microscopic images of MPNHm, the EB state of MPNHm appeared as a bright orange color, and the ES state of MPNHm appeared as a dark red color. These darkfield imaging results are consistent with the results of the absorbance spectra. Generally, objects can be said to have the color of light leaving their surfaces, that is, the human eye can perceive the color of objects by receiving the reflected

energy of light from the object. The absorbance spectra demonstrate that the energy of the valley is related to the reflected energy; in MPNHm, the valley energy of the EB state (pH 3–10) corresponds to 2.91 eV. This energy value represents a blue color, and for pH values 1 and 2, the valley energies match the color of each solution, respectively. In the darkfield microscopic images, on the other hand, the reflected light does not reach the eyepiece, but scattered light only reaches our eye; therefore, we can show the complementary color of the object in the darkfield microscopic images. As shown in the insets of Figure 2c, on the darkfield microscopic images, the color of MPNHm in the ES state (pH 1) is shown as a dark red color, which corresponds to the complementary color of green, and the color of MPNHm in the EB state (pH 10) is shown as a bright orange color, which corresponds to the complementary color of blue, respectively. Collectively, these results indicate that MPNHm can be doped with H+ ions and their counterions, and also suggests that the spectral changes and darkfield images of MPNHm can be used to determine the specific redox state of a biological system.

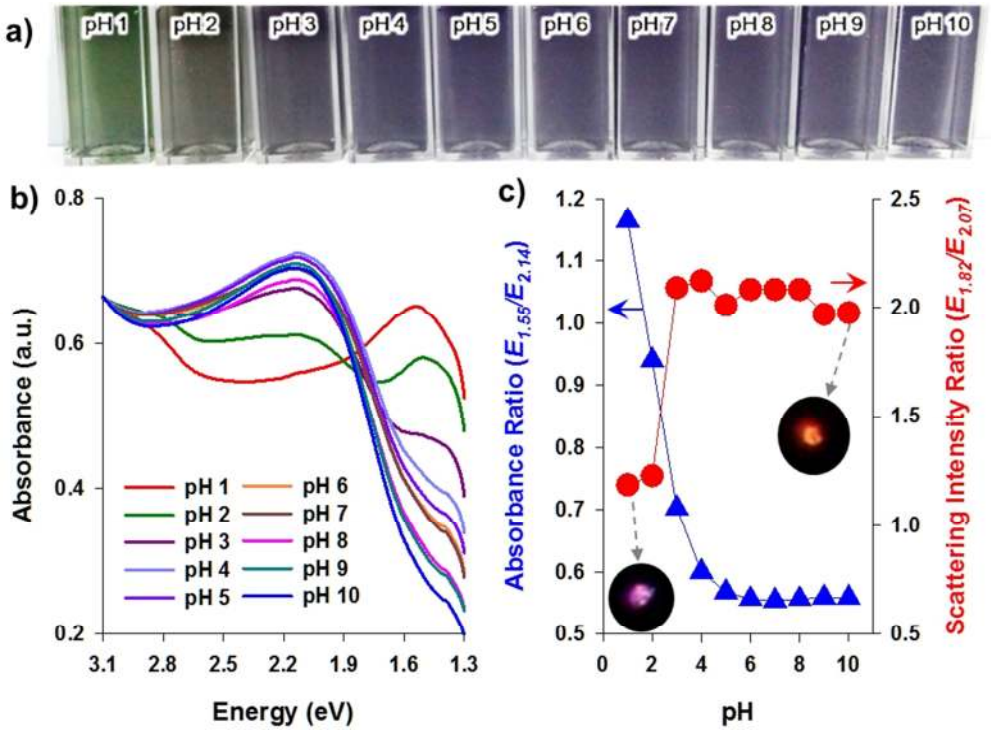

Figure III-3. A photograph of MPNHm in the indicated pH solutions. b) Absorbance spectra for MPNHm in pH 1–10. c) Absorbance ratio (E1.55/E2.14, triangle) and scattering intensity ratio (E1.82/E2.07, circle) for MPNHm as a function of pH. Insets represent light scattering images of MPNHm in the state of ES (pH 1) and EB (pH 10), respectively.

For the in vitro and in vivo MR imaging and redox sensing of cancer, hydrophobic MPNH was coated by MPNHm and dispersed in water. To study the redox-sensing ability, the MPNHm solution underwent repetitive doping and de-doping processes, and showed reversible green (ES) and blue (EB) changes (Figure III-4a). The hydrodynamic diameter showed no significant changes (MPNH: 62.2 ± 9.7 nm, MPNHm : 57.4 ± 2.3 nm) (Figure III-4b). X-ray diffraction (XRD) was used to obtain the structural information of Fe3O4 in MPNHm (Figure III-4c). The XRD patterns of MPNHm showed that MNPs contained in MPNHm were of a highly crystalline inverse spinel structure. The position diffraction peaks matched well with those of the magnetite powder. The magnetic hysteresis curves of MPNHm in the EB and ES states support the potential of MPNHm as an MR contrast agent (Figure III-4d). MPNHm in the EB state showed a superparamagnetic property with saturation magnetization at 3.8 emu/g. However, in the ES state, MPNHm shows a diamagnetic property, because MNPs contained in MPNHm dissolved and only PAni remained. To confirm the potential of MPNHm as an MR imaging contrast agent, solution MR imaging of MPNHm under EB, ES, and ES states after washing was performed (Figure III-4e). In the EB state, MPNHm successfully showed an increasing darkening contrast effect on T2 MR imaging with increasing iron concentrations, but no changes were seen on T1 MR imaging. In the ES state, MNPs contained in MPNHm were dissolved in acid; the iron ions showed no T2 contrast enhancing effect but showed significant brightening on T1 MR imaging. After washing in the ES state, MPNHm had no MNPs or iron ions, and showed no contrast enhancement effects on either T2 or T1 MR imaging. From these results, MPNH shows potential as a redox-sensing agent via reversible doping experiments, as well as potential as a MR imaging contrast agent via vibrating samples magnetometer (VSM) and solution MR imaging results.

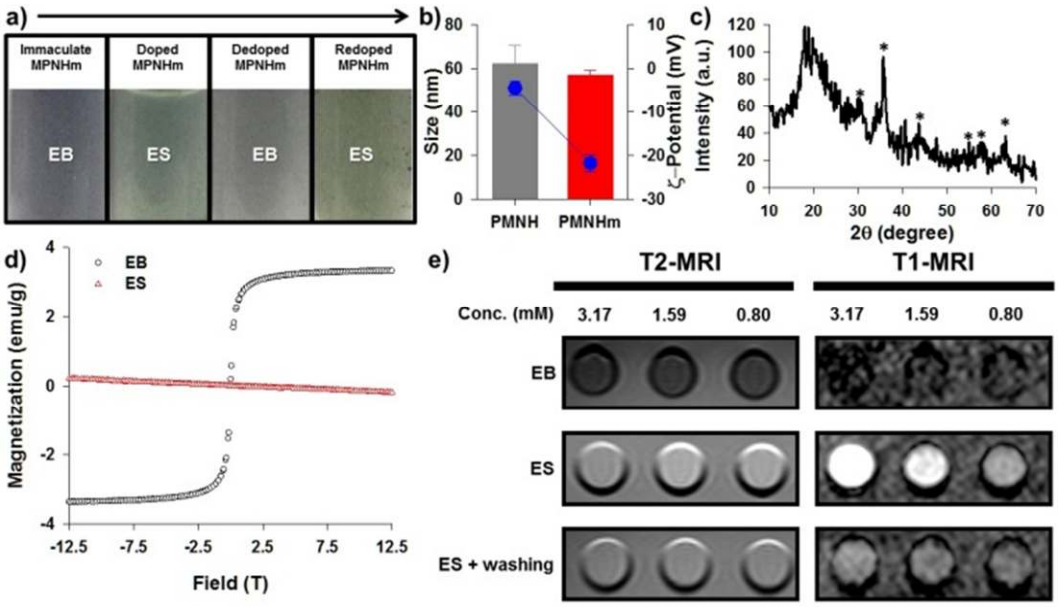

Figure III-4. a) A photograph of MPNHm solutions changing state. b) Size and zeta potential for MPNH and MPNHm. c) XRD pattern of MPNHm. The peaks of the Fe3O4 nanocrystal structure are marked with asterisks (*). d) Magnetic hyterisis loops for MPNHm in EB (black circle) and ES (red triangle) states. e) T2- and T1-MR images for MPNHm in EB, ES, and ES states after washing at the indicated concentrations.

To prepare the cancer MR imaging and redox-sensing probing based on MPNHm, an MT1-MMP-specific peptide was selected as a targeting moiety. MT1-MMP is a kind of specific metalloproteinase and plays a key role in cancer metastasis.[42, 43] An MT1-MMP-targeting peptide was designed to include a cysteine, which contains a thiol functional group and can be conjugated simply with the maleimidyl group of MPNHm at the proper pH.[44] MT1-MMP-targeting peptide-conjugated MPNH (MPNHm-P) was synthesized by simple mixing the MT1-MMP-targeting peptide and MPNHm. To evaluate the biocompatibility of MPNHm-P, cytotoxicity analysis was conducted (Figure III-5a). HT1080 and MCF7 cells were selected as the highly expressing MT1-MMP group and control group, respectively, because of their different

MT1-MMP expression levels.[45] The cytotoxicities of MPNHm-P in HT1080 and MCF7 cells were evaluated using the MTT assay for three different concentrations; the highest concentration, 3.17 mM, was diluted 10-fold twice. Neither HT1080 nor the MCF7 cells were damaged significantly by the treatment with the range of MPNHm-P concentrations used in this study. In Figure III-5b, images were obtained after a 24-h treatment of HT1080 and MCF7 cells with EB state-MPNHm-P. MPNHm-P was observed as the ES state color (green) in HT1080 cells, but in MCF7 cells, the EB state (blue) of MPNHm-P was maintained. This result demonstrates that MPNHm-P has an ability for cell-redox-state sensing and MT1-MMP targeting. To precisely examine the ability of MPNHm-P as a colorimetric probe at a microscopic scale, darkfield microscopy was carried out (Figure III-5c). In HT1080 cells, MPNHm-P bound to the surfaces of HT1080 cells and appeared in an ES state as in Figure 2c. In MCF7 cells, however, few or no MPNHm-P was observed, because MCF7 cells have a relatively lower expression level of MT1-MMP than HT1080 cells. The ES state of PAni allows PAni to receive biological dopants from biological systems, and these biological dopants (i.e.. H+ ions) are a representative material participating in redox reactions. In addition to this finding, PAni is also known as a nanoprobe that can sense various biological dopants, including one of the products of cancer metabolism, such as lactic acid or oxidative species, as well as H+ ions.7, 8 In HT1080 cells, these biological dopants from cancer cells may participate in changes in PAni from the EB to the ES state. The absorbance ratio (E1.55/E2.14) of HT1080 cells was also observed to be higher than in MCF7 cells, that is, MPNHm-P is in a ES-like state in HT1080 cells (Figure III-5d). These results show that MPNH is suitable for the sensing of the redox state of cancer cells using changes in its color via various methods (naked eye, spectrophotometer, and darkfield microscopic analysis). Collectively, the results of Figures 3 and 4 show that MPNHs are suitable as in vitro MR contrast agents and in vitro redox-sensing agents, because MPNHs have both properties of MNPs (MR contrast agent) and PAni (redox-sensing agent).

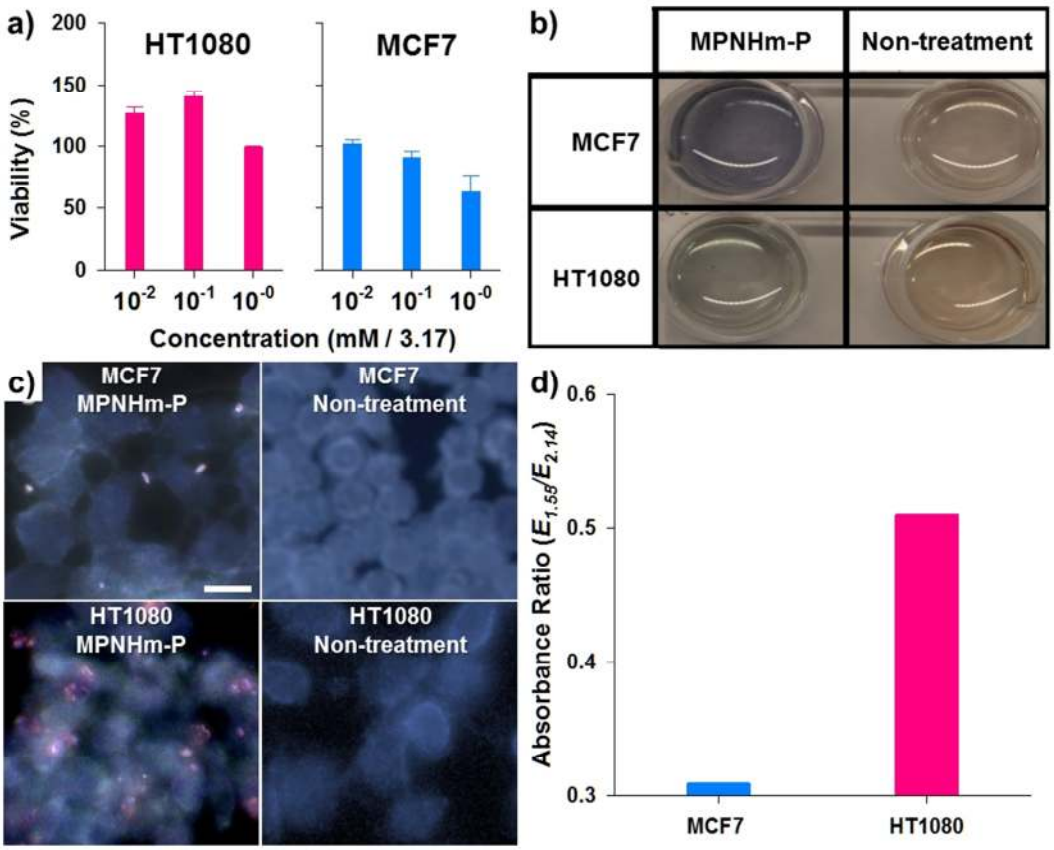

Figure III-5. a) Cell viability test of MPNHm-P in HT1080 and MCF7 cells. b) Photographs of MCF7 and HT1080 cells with or without MPNHm-P. c) Darkfield microscopic images of MCF7 (first raw) and HT1080 (second raw) cells with (the first column) or without (the second column) MPNHm-P. Scale bar is 10 μm. d) Absorbance ratios (E1.55/E2.14) for MCF7 and HT1080 cells treated with MPNHm-P.

To investigate the in vivo MT1-MMP-targeting ability of MPNHm-P using MR or optical imaging, we prepared xenograft mice model via the implantation of HT1080 cells at the proximal thigh. MR imaging of MT1-MMP-expressing fibrosarcomas was obtained after the injection of MPNHm-P into the tail vein of the mice (200 μg iron) (Figure III-6a, b). Before the injection of solution (pre-injection), each T2-weighted MR imaging of the tumor site appeared characteristically bright, with a low R2 value. Following the injection of MPNHm-P, we observed that the tumor sites showed darkened images caused by the presence of magnetic components. These results demonstrate that MPNHm-P was effectively targeted and bound to MT1-MMP in the tumor tissue. To quantify these results, MR imaging was evaluated quantitatively by a R2 relaxivity calculation (Figure III-6c). The R2 value increased in comparison with the pre-injection state. In vivo near infrared (NIR) imaging studies were also performed to evaluate the possibility of using MPNHm-P as a redox-sensing probe to detect HT1080 cells based on MT1-MMP expression (data not shown), and the total photon counts of NIR absorbance images in the tumor site were estimated (Figure III-6d). The total photon counts indicate the number of photons received from the reflected light of examined materials at the photon detector, and lower photon counts in absorbance images suggest that photons reaching the detector are also low; in other words, lower photon counts also indicate that the absorbance of the measured object is high in the absorbance image. As described in Figure 5d, after the MPNHm-P injection, the total photon counts were lower than those at pre-injection. This phenomenon indicates that reflected photons from the tumor site post-injection are lower than pre-injection, that is, the tumor site after MPNHm-P injection has a higher absorbance than pre-injection. To determine the precise regions detected by MPNHm-P, histological analysis was performed on the harvested HT1080 tumor tissues after MPNHm-P treatment and MR imaging. The dark purple region in the H&E-stained tissues clearly outlines the tumor (Fig. 5e), as the tumor tissue has dense, large cancer cells, with much nuclear material. The selective accumulation of MPNHm-P within the cells was verified using Prussian blue staining (Fig. 5f). iron ions from MPNHm-P bound to the HT1080 tumors combined with the ferrocyanide result in the formation of

a bright blue pigment called Prussian blue. These results demonstrate that HT1080 cells, which express high levels of MT1-MMP, were successfully targeted by MPNHm-P in vivo.

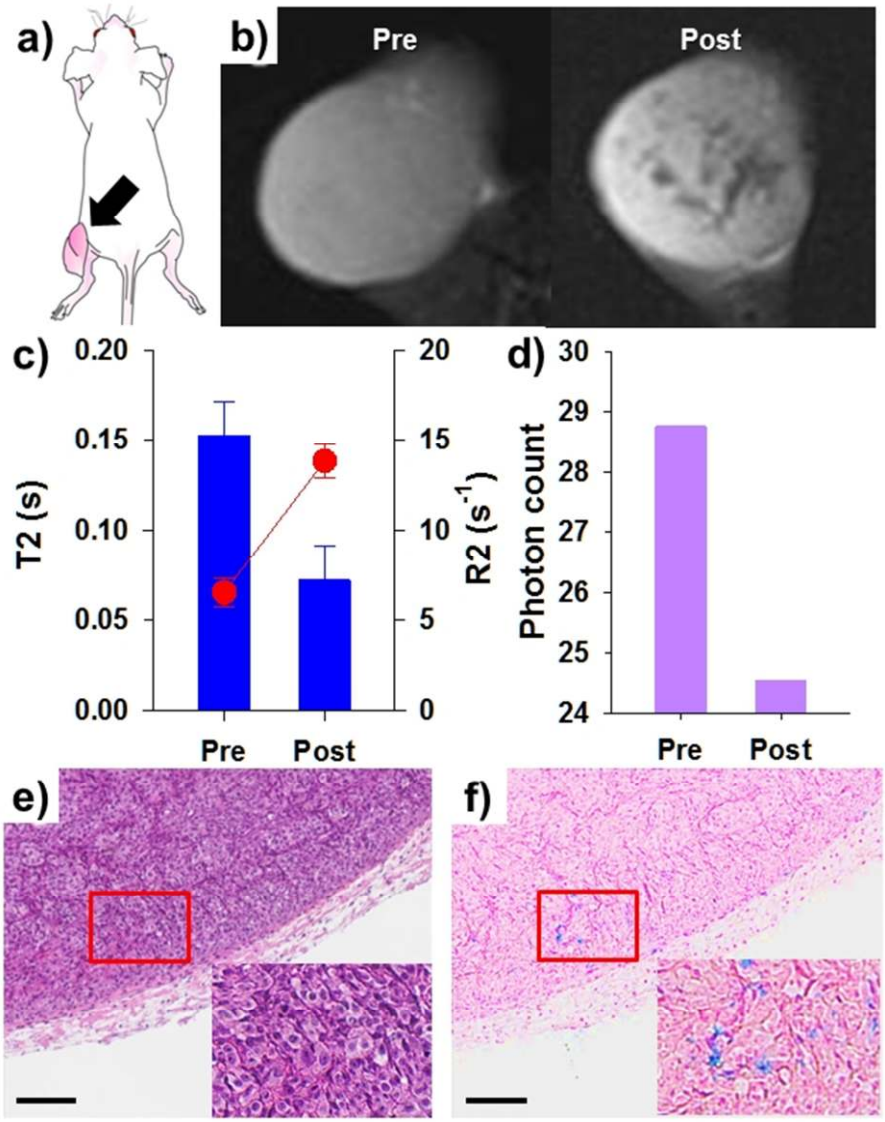

Figure III-6. a) A HT1080 xenograft mouse. The arrow points to the tumor site. b) In vivo T2-weighted MR images both pre-injection and 120 minutes after injection of MPNHm-P. c) T2 relaxation time (bar) and R2 for images in a). d) Photon counts corresponding to tumor specificity of MPNHm-P. e) H&E and f) Prussian blue staining images for tumor tissue sections. Scale bars are 100 μm. Insets are magnified images of the rectangular regions.

3.4. Conclusion

In conclusion, we designed a multifunctional nanohybrid that could act as an MR imaging contrast agent and redox-sensing agent; this nanohybrid was successfully used for dual modal imaging. The nanohybrid has a magnetic property as well as characteristics of polyaniline, and we verified that the nanohybrid could be used as an MR contrast agent and redox-sensing agent both in vitro and in vivo. We suggest that this nanohybrid could potentially lead to diagnoses of cancer by various methods, such as MR imaging or redox sensing.

Chapter IV

Conclusion

In conclusion, we designed the PAni-based nanocomplex so as to use for nanomedical technology. PAni-based polypex has satisfactory merit such as electro-chemical sensor. PANS performs the opto-electric sensor that it can detected the redox state using optical analysis, because it is able to play a mediator of electron transfer in enzyme-based redox reactions. On the other hand, MPNH is possible to use a multifunctional drug, because it is composed of magnetic nanoparticle and PAni. In addition, MPNH was conjugated with invasive cancer specific targetable peptide for markable therapeutic agent. In order to demonstrate MPNH as a multifunctional drug, in vitro and in vivo works show MR imaging potential and photothermal ablation capability of MPNH. In this study, we suggest a new way for utilization of PAni-based nanocomplex in the nanomedical technology. These researches are expect to develop of nanobiosensor for the biological science.

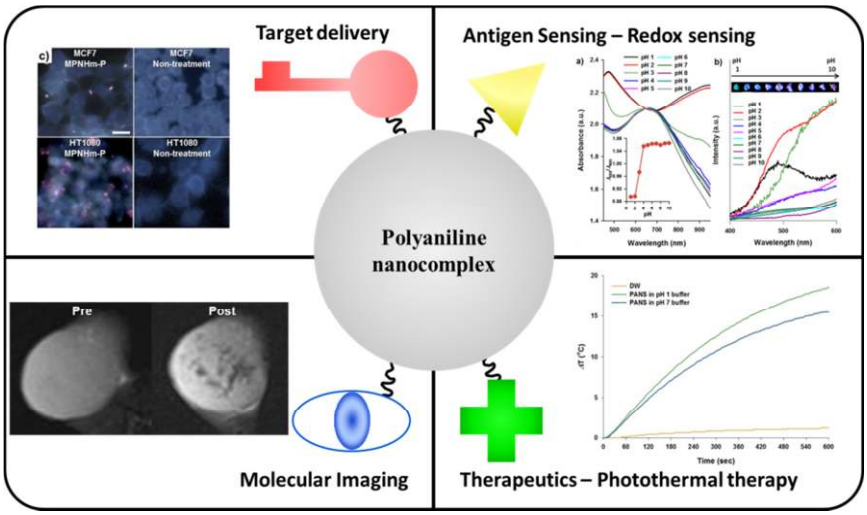

Figure IV-1. Polyaniline nanocomplex as a nanoprobe

Chapter V

References

1. Nel A, Xia T, Mädler L, Li N: **Toxic Potential of Materials at the Nanolevel.** *Science* 2006, **311:**622-627.
2. Salata O: **Applications of nanoparticles in biology and medicine.** *Journal of Nanobiotechnology* 2004, **2:**3.
3. Janib SM, Moses AS, MacKay JA: **Imaging and drug delivery using theranostic nanoparticles.** *Advanced Drug Delivery Reviews* 2010, **62:**1052-1063.
4. Pan L, He Q, Liu J, Chen Y, Ma M, Zhang L, Shi J: **Nuclear-Targeted Drug Delivery of TAT Peptide-Conjugated Monodisperse Mesoporous Silica Nanoparticles.** *Journal of the American Chemical Society* 2012, **134:**5722-5725.
5. Dan H, Eugene L, Minhee K, Seungyeon H, Bongjune K, Yeonji P, Young Han L, Yong-Min H, Seungjoo H, Jae-Ho C, et al: **Maleimidyl magnetic nanoplatform for facile molecular MRI.** *Nanotechnology* 2014, **25:**275102.
6. Freitas RA: **What is nanomedicine?** *Nanomedicine : nanotechnology, biology, and medicine* 2005, **1:**2-9.
7. Hong Y, Ku M, Heo D, Hwang S, Lee E, Park J, Choi J, Jung Lee H, Seo M, Jig Lee E, et al: **Molecular recognition of proteolytic activity in metastatic cancer cells using fluorogenic gold nanoprobes.** *Biosensors and Bioelectronics* 2014, **57:**171-178.
8. Lee G, Eom K, Park J, Yang J, Haam S, Huh Y-M, Ryu JK, Kim NH, Yook JI, Lee SW, et al: **Real-Time Quantitative Monitoring of Specific Peptide Cleavage by a Proteinase for Cancer Diagnosis.** *Angewandte Chemie International Edition* 2012, **51:**5837-5841.
9. Seung-Hyun Y, Dan H, Jinsung P, Sungsoo N, Jin-Suck S, Seungjoo H, Sahng Wook P, Yong-Min H, Jaemoon Y: **Role of surface charge in cytotoxicity of charged manganese ferrite nanoparticles towards macrophages.** *Nanotechnology* 2012, **23:**505702.

10. Vashist SK, Zheng D, Al-Rubeaan K, Luong JHT, Sheu F-S: **Advances in carbon nanotube based electrochemical sensors for bioanalytical applications.** *Biotechnology Advances* 2011, **29:**169-188.
11. Gao W, Uygun A, Wang J: **Hydrogen-Bubble-Propelled Zinc-Based Microrockets in Strongly Acidic Media.** *Journal of the American Chemical Society* 2011, **134:**897-900.
12. Chen D, Feng H, Li J: **Graphene Oxide: Preparation, Functionalization, and Electrochemical Applications.** *Chemical Reviews* 2012, **112:**6027-6053.
13. Sedó J, Saiz-Poseu J, Busqué F, Ruiz-Molina D: **Catechol-Based Biomimetic Functional Materials.** *Advanced Materials* 2013, **25:**653-701.
14. Valko M, Rhodes CJ, Moncol J, Izakovic M, Mazur M: **Free radicals, metals and antioxidants in oxidative stress-induced cancer.** *Chemico-Biological Interactions* 2006, **160:**1-40.
15. Kroemer G, Galluzzi L, Brenner C: *Mitochondrial Membrane Permeabilization in Cell Death.* 2007.
16. Valko M, Leibfritz D, Moncol J, Cronin MTD, Mazur M, Telser J: **Free radicals and antioxidants in normal physiological functions and human disease.** *The International Journal of Biochemistry & Cell Biology* 2007, **39:**44-84.
17. Yang J, Choi J, Bang D, Kim E, Lim E-K, Park H, Suh J-S, Lee K, Yoo K-H, Kim E-K, et al: **Convertible Organic Nanoparticles for Near-Infrared Photothermal Ablation of Cancer Cells.** *Angewandte Chemie International Edition* 2011, **50:**441-444.
18. Choi J, Hong Y, Lee E, Kim M-H, Yoon D, Suh J, Huh Y, Haam S, Yang J: **Redox-sensitive colorimetric polyaniline nanoprobes synthesized by a solvent-shift process.** *Nano Research* 2013, **6:**356-364.
19. Cao Y, Smith P, Heeger AJ: **Spectroscopic studies of polyaniline in solution and in spin-cast films.** *Synthetic Metals* 1989, **32:**263-281.
20. Chen X, Chen Z, Zhu J, Xu C, Yan W, Yao C: **A novel H2O2 amperometric biosensor based on gold nanoparticles/self-doped polyaniline nanofibers.** *Bioelectrochemistry* 2011, **82:**87-94.
21. Tamboli MS, Kulkarni MV, Patil RH, Gade WN, Navale SC, Kale BB: **Nanowires of silver–polyaniline nanocomposite synthesized via in situ polymerization and its novel functionality as an antibacterial agent.** *Colloids and Surfaces B: Biointerfaces* 2012, **92:**35-41.
22. Jena BK, Raj CR: **Synthesis of Flower-like Gold Nanoparticles and Their**

Electrocatalytic Activity Towards the Oxidation of Methanol and the Reduction of Oxygen. *Langmuir* 2007, **23:**4064-4070.

23. Li C, Su Y, Zhang S, Lv X, Xia H, Wang Y: **An improved sensitivity nonenzymatic glucose biosensor based on a CuxO modified electrode.** *Biosensors and Bioelectronics* 2010, **26:**903-907.
24. Liu W, Kumar J, Tripathy S, Senecal KJ, Samuelson L: **Enzymatically Synthesized Conducting Polyaniline.** *Journal of the American Chemical Society* 1998, **121:**71-78.
25. Li D, Huang J, Kaner RB: **Polyaniline Nanofibers: A Unique Polymer Nanostructure for Versatile Applications.** *Accounts of Chemical Research* 2008, **42:**135-145.
26. Ma Y, Zhang J, Zhang G, He H: **Polyaniline Nanowires on Si Surfaces Fabricated with DNA Templates.** *Journal of the American Chemical Society* 2004, **126:**7097-7101.
27. Anilkumar P, Jayakannan M: **Hydroxyl-Functionalized Polyaniline Nanospheres: Tracing Molecular Interactions at the Nanosurface via Vitamin C Sensing.** *Langmuir* 2008, **24:**9754-9762.
28. Niu Z, Yang Z, Hu Z, Lu Y, Han CC: **Polyaniline–Silica Composite Conductive Capsules and Hollow Spheres.** *Advanced Functional Materials* 2003, **13:**949-954.
29. Jiang S, Chen J, Tang J, Jin E, Kong L, Zhang W, Wang C: **Au nanoparticles-functionalized two-dimensional patterned conducting PANI nanobowl monolayer for gas sensor.** *Sensors and Actuators B: Chemical* 2009, **140:**520-524.
30. Ding H, Zhu C, Zhou Z, Wan M, Wei Y: **Monodispersed and Oriented Microspheres of Polyaniline.** *Macromolecular Chemistry and Physics* 2006, **207:**1159-1165.
31. Yang J, Lee C-H, Ko H-J, Suh J-S, Yoon H-G, Lee K, Huh Y-M, Haam S: **Multifunctional Magneto-Polymeric Nanohybrids for Targeted Detection and Synergistic Therapeutic Effects on Breast Cancer.** *Angew Chem Int Ed* 2007, **46:**8836-8839.
32. Lee J, Yang J, Ko H, Oh S, Kang J, Son J, Lee K, Lee SW, Yoon HG, Suh JS, et al: **Multifunctional Magnetic Gold Nanocomposites: Human Epithelial Cancer Detection via Magnetic Resonance Imaging and Localized Synchronous Therapy.** *Adv Funct Mater* 2008, **18:**258-264.

33. Park H, Yang J, Seo S, Kim K, Suh J, Kim D, Haam S, Yoo K-H: **Multifunctional Nanoparticles for Photothermally Controlled Drug Delivery and Magnetic Resonance Imaging Enhancement.** *Small* 2008, **4:**192-196.
34. Park H, Yang J, Lee J, Haam S, Choi I-H, Yoo K-H: **Multifunctional Nanoparticles for Combined Doxorubicin and Photothermal Treatments.** *ACS Nano* 2009, **3:**2919-2926.
35. Goodwill PW, Saritas EU, Croft LR, Kim TN, Krishnan KM, Schaffer DV, Conolly SM: **X-Space MPI: Magnetic Nanoparticles for Safe Medical Imaging.** *Adv Mater* 2012, **24:**3870.
36. Shi L, Xiao Y, Willner I: **Electrical contacting of glucose oxidase by DNA-templated polyaniline wires on surfaces.** *Electrochem Commun* 2004, **6:**1057.
37. Wolter A, Rannou P, Travers JP, Gilles B, Djurado D: **Model for aging in HCl-protonated polyaniline: Structure, conductivity, and composition studies.** *Phys Rev B* 1998, **58:**7637.
38. Ueda S, Nakamura H, Masutani H, Sasada T, Yonehara S, Takabayashi A, Yamaoka Y, Yodoi J: **Redox Regulation of Caspase-3(-like) Protease Activity: Regulatory Roles of Thioredoxin and Cytochrome c.** *J Immunol* 1998, **161:**6689.
39. Winterbourn CC, Hampton MB: **Thiol chemistry and specificity in redox signaling.** *Free Radic Biol Med* 2008, **45:**549.
40. Mavridou DAI, Saridakis E, Kritsiligkou P, Goddard AD, Stevens JM, Ferguson SJ, Redfield C: **Oxidation State-dependent Protein-Protein Interactions in Disulfide Cascades.** *J Biol Chem* 2011, **286:**24943.
41. Wang Y, Yang J, Yi J: **Redox Sensing by Proteins: Oxidative Modifications on Cysteines and the Consequent Events** *Antioxid Redox Signal* 2012, **16:**649.
42. Kajita M, Itoh Y, Chiba T, Mori H, Okada A, Kinoh H, Seiki M: **Membrane-Type 1 Matrix Metalloproteinase Cleaves Cd44 and Promotes Cell Migration.** *J Cell Biol* 2001, **153:**893.
43. Wolf K, Mazo I, Leung H, Engelke K, von Andrian UH, Deryugina EI, Strongin AY, Bröcker E-B, Friedl P: **Compensation mechanism in tumor cell migration: mesenchymal–amoeboid transition after blocking of pericellular proteolysis.** *J Cell Biol* 2003, **160:**267.
44. Ghosh SS, Kao PM, McCue AW, Chappelle HL: **Use of maleimide-thiol coupling chemistry for efficient syntheses of oligonucleotide-enzyme conjugate hybridization probes.** *Bioconjug Chem* 1990, **1:**71-76.

45. Rozanov DV, Deryugina EI, Ratnikov BI, Monosov EZ, Marchenko GN, Quigley JP, Strongin AY: **Mutation Analysis of Membrane Type-1 Matrix Metalloproteinase (MT1-MMP): THE ROLE OF THE CYTOPLASMIC TAIL CYS574, THE ACTIVE SITE GLU240, AND FURIN CLEAVAGE MOTIFS IN OLIGOMERIZATION, PROCESSING, AND SELF-PROTEOLYSIS OF MT1-MMP EXPRESSED IN BREAST CARCINOMA CELLS.** *J Biol Chem* 2001, **276:**25705.

Abstract (in Korean)

공액 고분자 기반 나노 복합체를 이용한 바이오 나노프로브

황승연

나노 메디컬 협동과정

연세대학교 대학원

최근, 공액 고분자의 산화, 환원 상태에 따라 발생하는 광전자적 특성의 가변성을 이용하여 센서로써 이용하는 연구가 활발하게 진행되고 있다. 그 중에서도 폴리아닐린은 합성이 쉬우며, 높은 전기 전도도를 갖고, 광전자적 특성의 조절이 용이하다는 점에서 주목받고 있다. 특히 폴리아닐린 복합체는 전자 전이 매개체로써 작용이 가능하기에 효소 기반의 산화 환원 반응을 전기 화학적으로 감지하는 센서로써 이용이 가능하며, 나노 크기의 폴리아닐린 입자는 생물학적인 도핑에 의해 색상을 변화시키는 특성을 가진다는 점에서 더욱 효용성이 크다. 본 논문에서는 폴리아닐린의 나노복합체의 형성을 통해 생의학적 나노프로브로써의 활용에 대해 고찰하였다.

본 논문에서는 폴리아닐린 기반 나노프로브로의 이용방안으로 폴리아닐린의 다공성 나노구조체와 자기 공명 영상법의 조영제로써 이용 가능한 자성 나노입자와의 복합체를 형성시켜 다중 진단 시약으로 이용하는 방법을 고안하였다. 먼저, 폴리아닐린 다공성 나노구조체는 폴리아닐린을 다양한 용매와 혼합, 가열하여

표면적이 크고, 표면이 매끄럽지 않은 구조로 형성되며 나타나는 광학적 특성의 변화를 이용하여 광학기반의 나노프로브로의 가능성을 모색한 것이다. 다공성 구조로 인해 생물학적 도핑에 의한 산화 환원 상태를 민감하게 감지하며, 산란 분광법, 라만 분광법 등의 다양한 방법으로 생체 활성 나노프로브로의 가능성을 확인하였다. 또한, 해부학적 영상을 통해 질병의 상세한 진단을 위해 많이 사용되고 있는 자기 공명 영상 기법과의 연계하기 위해 자성 나노 입자의 복합체를 형성시켜 자성 폴리아닐린 나노혼성체를 제작하였다. 자성 폴리아닐린 나노혼성체는 열 분해 방법으로 제작되어 암 표적화 리간드 결합체가 처리된 양친매성 계면 활성제로 표면처리 되어, 특정 질환에 표적적으로 작용하는 바이오마커와 결합시켰으며, 이를 이종이식 생쥐 모델을 이용하여 표적성과 자기 공명 영상 진단제로의 효능을 확인하였다.

결론적으로, 본 논문에서는 폴리아닐린을 생물 의학적인 센서로써 이용하기 위한 나노 복합 재료를 설계하고, 광전자적 특성을 이용하여 생물학적 도핑에 의한 산화 환원 상태를 검출하고, 자기 공명 영상을 통해 표적성을 갖는 다 기능성 나노프로브의 가능성을 확인하였다. 이러한 공액 고분자 기반 나노복합체를 이용한 바이오 나노프로브는 질병의 정확한 진단과 치료 경과를 관측하는 진단제로의 이용이 가능하며, 공액 고분자 소재를 의학적으로 이용하는 새로운 이용방법을 제시할 것으로 기대된다.

핵심되는 말: 폴리 아닐린 • 나노프로브 • 나노입자 • 핵 자기 공명 영상 • 자성 나노 입자 • 바이오마커 • 공액 고분자 • 진단